Femtochemistry at Metal Surfaces: Nonadiabatic Reaction Dynamics

Christian Frischkorn* and Martin Wolf*

Freie Universität Berlin, Fachbereich Physik, Arnimallee 14, 14195 Berlin, Germany

Received June 13, 2006

Contents

1. Introduction

Femtochemistry addresses fundamental processes of chemical reaction dynamics such as bond formation and breaking, which occur typically on a femtosecond time scale (1 fs = 10^{-15} s). Experimental studies with femtosecond time resolution have only become possible by the development of lasers with respectively ultrashort pulse duration, which in turn had a strong impact on further investigations. Pioneered by Zewail and co-workers (e.g., see refs 1 and 2), femtochemistry has led to enormous progress in the understanding and even control of chemical reactions in the *gas and solution phases* over the past decades. However, a comparable level of sophistication in the analysis of *surface* chemical reactions has not been achieved due to the additional complexity of energy dissipation channels introduced by the presence of a solid interface interacting with the reactants. Reactive processes at surfaces are of fundamental importance for technological applications such as heterogeneous catalysis. Here, metals are often investigated as model substrates since the interaction of the adsorbed reaction partners with the substrate may cause a favorable energy landscape, for example, a reduced reaction barrier compared with the gas phase. Moreover, the ability to bring the reactants on a surface, like on a template, into close proximity provides additional control of the reaction dynamics. On the other hand, coherent control schemes, which exploit the phase of the exciting laser light field, are expected to fail in photoinduced surface processes due to ultrafast dephasing caused by coupling to the underlying substrate.

A key concept of chemical reaction dynamics relies on the Born−Oppenheimer approximation whereby electrons are assumed to follow the nuclear motion instantaneously. The dynamics of a chemical reaction are described by the evolution of the reactants to the product state on a Born−Oppenheimer potential energy surface (PES), on which (either in the ground or an excited state) the reaction evolves electronically adiabatically.[3,4] Thereby, nonadiabatic coupling effects between nuclear motions and electronic degrees of freedom are neglected. This, however, represents a valid approximation only if the involved PESs do not approach each other significantly. By contrast, in cases such as conical intersections, crossing of two PESs at a certain nuclear configuration leads to coupling between different electronic configurations.[5] At metal surfaces, where a whole manifold of PESs exists, which are coupled by a continuum of electron−hole pair excitations in the substrate, such nonadiabatic coupling between electronic and nuclear degrees of freedom becomes even more relevant.[6] Despite this fact, the Born−Oppenheimer approximation is often successfully applied to describe surface reaction dynamics on the ground state PES. However, for highly exothermic reactions on metal surfaces, there is already experimental evidence that the assumption of uncoupled nuclear and electronic degrees of freedom may break down and that energy is transferred from the reactants to electronic excitations in the substrate (e.g., electron−hole pairs or plasmons). Well-known examples are the emission of exoelectrons or surface chemiluminescence during the oxidation of alkali metal surfaces.[7] Moreover, the excitation of hot electrons has been observed during adsorption of various gases on thin metal films by detection of chemicurrents across the Schottky barrier on an n-type silicon

* E-mail addresses: christian.frischkorn@physik.fu-berlin.de; wolf@physik.fu-berlin.de.

10.1021/cr050161r CCC: $59.00
Published on Web 09/21/2006

Christian Frischkorn received his Diploma in Physics from the Technical University of Darmstadt in 1993 working on coherent Raman spectroscopy at the mechanical engineering department. After 6 months at the East China Normal University in Shanghai in the quantum optics laboratory led by Zu-Geng Wang and Hui-Rong Xia, he returned to Germany and did research on cluster photodissociation under the supervison of Udo Buck at the Max-Planck-Institut für Strömungsforschung in Göttingen. He received his Ph.D. in 1997 and spent then 2 years as a Leopoldina postdoctoral fellow at UC Berkeley in Dan Neumark's group working on ultrafast electron solvation dynamics in clusters. In late 2000, he joined the group of Martin Wolf at the Freie Universität Berlin. Christian, who is currently finalizing his habilitation degree, is interested in ultrafast laser-induced physics and chemistry on surfaces and also in charge-carrier dynamics observed with time-resolved terahertz spectroscopy.

Martin Wolf received his Ph.D. degree in physics in 1991 from the Freie Universität Berlin, Germany, for his work on photochemistry at metal surfaces performed under the direction of Prof. Gerhard Ertl at the Fritz-Haber-Institut, Berlin. After a postdoctoral period in Austin, Texas, with Prof. Mike White, he set up a laboratory for femtosecond surface spectroscopy at the Fritz-Haber-Institut in Berlin. He was also a visiting scientist at IBM Yorktown Heights with Prof. Tony Heinz. In 2000, he was appointed as a full professor for experimental physics at the Freie Universität Berlin. His work is devoted to the dynamics of elementary excitations in solids and at interfaces as well as ultrafast reactions and conformational changes at surfaces. Recent efforts address also electron dynamics in highly correlated materials, ferromagnets, and metallic quantum well states. These studies employ a broad spectrum of time-resolved techniques including time-resolved photoelectron spectroscopy, nonlinear optics at interfaces, and terahertz time-domain spectroscopy.

substrate.[8] Further examples of nonadiabatic effects at metal surfaces include energy dissipation by scattering of highly vibrationally excited molecules,[6] vibrational energy relaxation,[9] or dissociative adsorption.[10]

In surface femtochemistry, nonadiabatic coupling between photoexcited electron−hole pairs in the substrate and adsorbate vibrational degrees of freedom provides the driving force for femtosecond-laser-induced chemical reactions.[11] Absorption of a femtosecond light pulse by a metal substrate generates a transient nonequilibrium distribution of hot electrons, which thermalize by ultrafast electron−electron scattering and lead to an electron temperature exceeding the lattice temperature by several thousand kelvin on a subpicosecond time scale.[12] Coupling of this electronic transient to adsorbate vibrational degrees of freedom will eventually cause processes such as desorption[13,14] or reactions between coadsorbed species.[15−18] Because these reactive processes compete with various energy dissipation channels to electronic and phononic degrees of freedom of the underlying substrate, the reaction dynamics occur predominantly on the ground-state PES.

Unlike in gas-phase femtochemistry, where over the years several profound review articles (e.g., ref 2 and references therein) and books (e.g., ref 1) have appeared, only two articles dedicated solely to femtosecond *surface* chemistry have been published more than a decade ago.[11,19] Other review articles in the field address surface photochemistry more generally and focus on specific aspects such as state-resolved dynamics,[20] laser-stimulated desorption from oxides,[21] or wave packet dynamics of the adsorbate−metal bond.[22] Therefore, it is the aim of this paper to specifically review the progress in surface femtochemistry in the last decade and to discuss the current status and relevance of nonadiabatic surface processes in a broader context. The review is organized as follows. In section 2, the basic concepts of femtosecond-laser excitation and subsequent energy flow are introduced. This is followed by an overview of the experimental techniques and instrumentation necessary to perform these studies. Section 4 covers a brief history of surface femtochemistry including the main achievements since the first report in this field in 1990.[23] In the main portion, section 5, the various experimental observables in surface femtochemistry are explained, and their interpretation for the underlying reaction dynamics is discussed. Section 6 comprises the recent developments in surface femtochemistry in connection to related fields and its impact on them. Conclusions are finally given in section 7.

2. Basic Concepts

Surface femtochemistry is initiated by ultrashort-laser pulse excitation of an adsorbate-covered metal surface. The subsequent elementary processes can be grouped into two parts. The first area covers processes within the substrate where the laser pulse is absorbed and the energy dissipated. These processes are crucial for the evolving reaction dynamics, since reactions mediated by the underlying substrate typically dominate (i.e., direct optical absorption is mostly negligible in atomically thin adsorbate layers). The second field comprises the subsequent energy transfer to the adsorbate system, which involves the coupling of electronic and nuclear degrees of freedom. Figure 1, top panel, illustrates the energy flow among the different subsystems and gives characteristic time constants for the respective energy transfer. In the following subsections, the processes of intrasubstrate and substrate−adsorbate energy transfer are expanded in more detail.

2.1. Energy Transfer Processes in the Metal Substrate

From a simplified point of view, a metal substrate consists of two heat baths, the ion cores (lattice) and the surrounding electron gas. Excitations of either of these subsystems, that

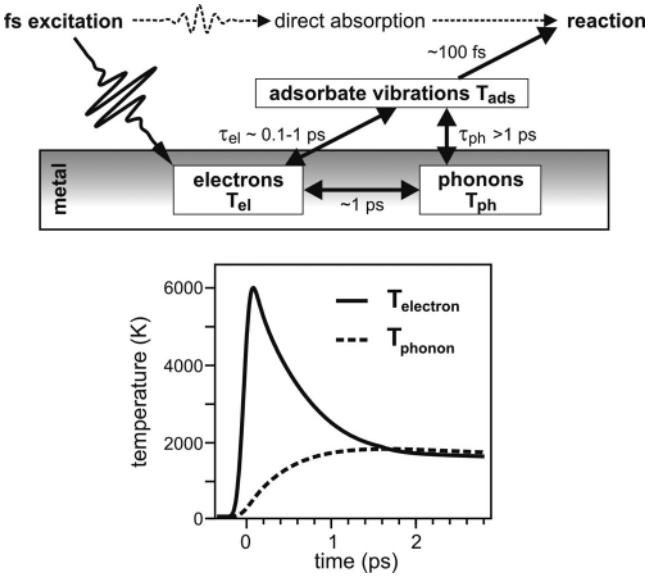

Figure 1. (top) Schematic diagram of the energy flow at metal surfaces after femtosecond-laser excitation. Time scales of energy exchange among various subsystems are discussed in the text. While direct absorption in the adsorbate can be neglected in thin atomic or molecular layers, the femtosecond-laser radiation excites the electronic system of the substrate, which then equilibrates with the lattice phonons on the order of the electron−phonon coupling time. Surface reactions can be driven either by electronic coupling or by lattice phonons. Reproduced from ref 64, Copyright 2002, with permission from World Scientific Publishing Co. Pte. Ltd., Singapore. (bottom) Typical temperature transients for the electron and phonon heat baths with temperatures T_{el} and T_{ph}, respectively, calculated with the two-temperature model[12] here for Ru as the substrate metal. The parameters of the exciting laser pulse are 120 fs and 50 mJ/cm^2 at 800 nm center wavelength.

is, collective lattice vibrations (phonons) and electron gas excitations, respectively, constitute the energy content of the substrate. Consequently, the degree of excitation can be described by two population distributions, which are characterized (in the limit of thermalized distributions) by the two temperatures of their respective distribution functions, T_{el} for the electronic temperature and T_{ph} for the phonon temperature. In thermal equilibrium or when the substrate is heated conventionally (i.e., not by femtosecond-laser excitation), equal temperatures for both heat baths prevail; $T_{el} = T_{ph}$ due to electron−phonon coupling with a typical equilibration time in the picosecond (ps) range (see Figure 1, top panel). However, excitation with a femtosecond-laser pulse will drive the system out of equilibrium. The pulse energy is deposited into the electron system, and due to the small heat capacity of the electrons (compared to the lattice), T_{el} rises within the pulse width to levels far above the melting point of the lattice. This electronic excitation energy is then dissipated either by electron diffusion into the bulk or by energy transfer (cooling) into the phonon subsystem via electron−phonon coupling.[24,25] This gives rise to an increase of the phonon temperature, T_{ph}, however, on a much slower time scale than the electronic response. Within a time span of approximately the electron−phonon coupling time of the substrate, both the electron and phonon heat baths equilibrate. Figure 1, bottom panel, shows typical transients for T_{el} and T_{ph} exemplarily for ruthenium obtained with the so-called two-temperature model (2TM) explained below. A pronounced thermal nonequilibrium between both subsystems with $T_{el} \gg T_{ph}$ exists for the first 1−2 ps after excitation. The 2TM has been established to quantitatively describe such a system of two coupled heat baths using the following coupled differential equations:[12,26,27]

$$C_{el}\frac{\partial}{\partial t}T_{el} = \overbrace{\nabla_z(\kappa\nabla_z T_{el})}^{\text{therm.diffusion}} - \overbrace{g(T_{el}-T_{ph})}^{\text{el-ph.coupling}} + \overbrace{S(z,t)}^{\text{opt.excitation}} \quad (1)$$

$$C_{ph}\frac{\partial}{\partial t}T_{ph} = g(T_{el}-T_{ph}) \quad (2)$$

where $C_{el} = \gamma T_{el}$ is the electron heat capacity with γ as the corresponding specific heat.[28] The heat capacity of the lattice C_{ph} typically is taken from the Debye model, which is explained in detail in solid-state physics textbooks (e.g., ref 29). Finally, κ and g denote the thermal conductivity and the electron−phonon coupling constant, respectively. Heat conduction by phonons can be neglected in metals because the mean velocities of electrons and phonons enter the heat conductivity quadratically and the Fermi velocity is much larger than the speed of sound.[29] The temperature dependence of the electronic thermal conductivity is described within the Sommerfeld approximation by $\kappa = \kappa_0(T_{el}/T_{ph})$.[30] Since the beam diameter of the exciting laser pulse on the surface is much larger than the electron diffusion length, lateral diffusion can be neglected resulting in the reduced dimensionality of eq 1, z being the distance along the surface normal. The energy of the laser excitation enters the source term in eq 1 as

$$S(z,t) = (1-R)I(t)\delta^{-1}\exp\left(-\frac{z}{\delta}\right) \quad (3)$$

Here, δ, R, and $I(t)$ stand for the optical penetration depth, the substrate reflectivity, and the time profile of the laser intensity, respectively.

The whole model described so far relies on the applicability of the temperature concept to each of the subsystems. However, initially, the absorption of the laser photons definitely creates a nonequilibrium distribution of electrons and holes, which *cannot* be described by an electron temperature, T_{el}, immediately after optical excitation. Yet the evolving rapid electron−electron scattering leads to a thermalized but still hot electron distribution with a genuine T_{el} on a time scale comparable to the laser pulse duration as illustrated in Figure 2a,b. Hence, based on the assumption of rapid thermalization, the 2TM outlined above is frequently applied to describe femtosecond-laser-induced processes in a metal substrate prior to the subsequent surface reactions. This seems justified by the finding that in time-resolved experiments on gold at low excitation densities, electron thermalization occurs within several hundreds of femtoseconds but becomes much faster at higher fluences.[31,32] In addition, for certain metals such as ruthenium, the shorter electron−electron scattering time compared with gold due to the higher density of states around the Fermi level[33] should facilitate an even more rapid thermalization within the time scale of laser pulse absorption. Despite this reasoning, however, there exists evidence that in specific systems the initially created *non*equilibrium electrons may also contribute to the experimental outcome of a surface reaction and should not be neglected in all circumstances.[34] The notion that only the resulting hot Fermi−Dirac electron distribution after thermalization irrespective of the photon energy used for excitation determines the reaction yield is insufficient to

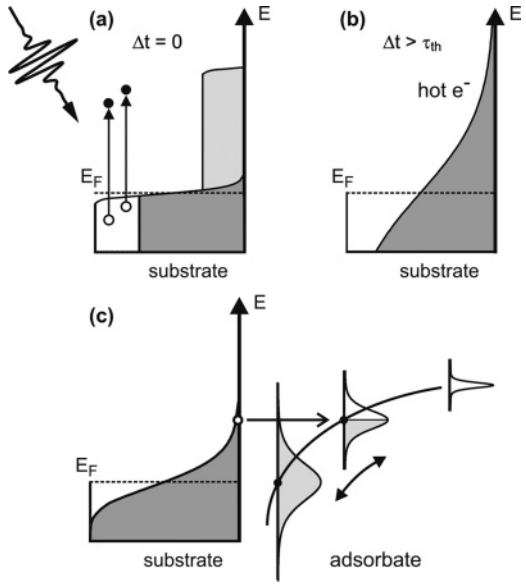

Figure 2. Optical excitation, electron thermalization, and vibrational damping by electronic friction: (a) at $\Delta t = 0$, when the femtosecond-laser pulse excites the metal electrons, a nonequilibrium population distribution is generated; (b) after thermalization, a hot electron distribution is attained with a high-reaching energy tail; (c) from an exemplary electronic (equilibrium) distribution, an adsorbate-derived affinity level (middle) may be populated by substrate electrons. Adsorbate motion is initiated through a changed charge distribution. The resulting electron flow back and forth between metal and adsorbate is subject to damping (friction). Note that in the case of high-lying adsorbate resonances (right), this charge-transfer channel may not be open.

understand certain excitation wavelength-dependent experiments, as will be further discussed in section 5.4.

How such nonthermalized electrons manifest themselves experimentally can be probed directly by time-resolved photoemission spectroscopy (TRPES). In such pump−probe experiments, the ejected photoelectrons are detected and analyzed according to their kinetic energy. As an example, Figure 3, top panel, shows the TRPES intensity from a D_2O-covered Ru surface as a function of the energy of the intermediate state, which is transiently populated by the pump pulse, with respect to the Fermi level. As seen for a time delay of $\Delta t = 100$ fs, the obtained electron distribution significantly deviates from a Fermi−Dirac distribution with a certain electron temperature. Moreover, based on these experiments, it was recently found that the conventional 2TM overestimates the energy content of the lattice in the surface-near region at least for relatively low excitation densities (absorbed fluences ≤ 0.6 mJ/cm^2). The bottom panel of Figure 3 displays the time profile of the energy density in the electron system extracted from TRPES spectra, which clearly differs from 2TM predictions. An extension to this model, which accounts for the initially nonthermalized electrons after the excitation and for ballistic transport, well reproduces the experimental data.[35,36] Whether the new extended temperature model by Lisowski et al.[35] might alter some aspects of previous experiments and their interpretation based on standard two-temperature modeling still needs to be clarified. However, the significantly higher excitation densities usually applied in surface femtochemistry and the resulting faster thermalization due to rapid electron−electron scattering are believed to be the reason that the ordinary 2TM used in most cases is still adequate and yields excellent agreement with the experiment (see refs 17, 18, 37, and 38).

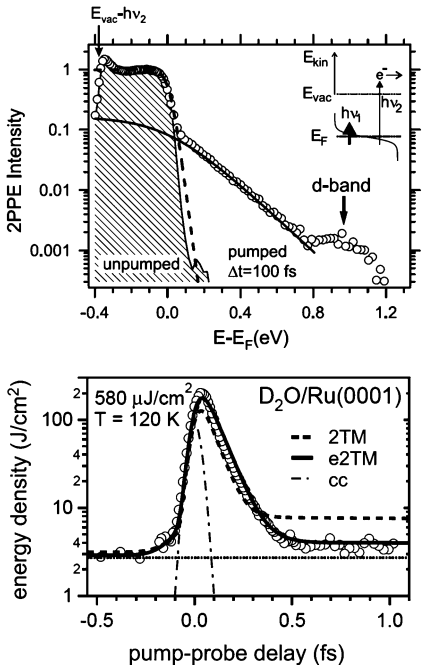

Figure 3. (top) Electron distribution after femtosecond-laser excitation measured with two-photon photoemission. 2PPE spectra of 1 bilayer (BL) D_2O/Ru(001) both unpumped (hatched area underneath the thin solid line) and pumped (open circles, pump−probe delay $\Delta t = 100$ fs, absorbed fluence 580 μJ/cm^2). The semilogarithmically plotted spectra are normalized to unity at $E - E_F = -150$ meV. The dashed line is a fitted Fermi−Dirac distribution to the pumped spectrum with $T_{el} = 225$ K. The deviation from such a distribution is demonstrated by the thick solid line, which approximates the nonthermal part of the excited electron distribution. The inset sketches the 2PPE principle with, in the present case, pump and probe photon energies, $h\nu_1$ and $h\nu_2$, of 1.55 eV (s-polarized) and 4.58 eV (p-polarized), respectively. Reprinted with permission from ref 35. Copyright 2004 Springer-Verlag. (bottom) Temporal evolution of the energy density extracted from the 2PPE spectra above for the photoexcited 1 BL D_2O/Ru(001) system. The dashed line marks the outcome of the two-temperature model (2TM), ref 12, while the solid line originates from an extended 2TM (e2TM), which incorporates ballistic transport and nonthermal electrons (for details, see ref 35). The latter are taken into account by reducing the electron−phonon coupling strength for a certain portion of the entire electron system (i.e., the photoexcited electrons). The dash−dotted line indicates the cross correlation of pump and probe pulse reflecting the inherent time resolution of the experiment.

2.2. Substrate–Adsorbate Coupling

Each of the substrate's energy reservoirs described in the previous section, the electron and phonon subsystem, may couple energy independently into the adsorbate system, which undergoes reaction after accumulation of sufficient energy in the coordinate relevant to the reaction (see Figure 1). The energy transfer from the initially excited electronic degrees of freedom of the substrate to the nuclear motion of the reactants occurs either directly through electronically nonadiabatic substrate−adsorbate coupling or indirectly via equilibration with the lattice and subsequent coupling to the adsorbate. In surface femtochemistry, two conceptually different frameworks have been developed to describe these transfer mechanisms. One approach treats the energy transfer in terms of friction[39,40] with frictional coefficients $\eta_x = 1/\tau_x$, $x =$ ph,el for both phonons and electrons, which determine how fast energy flows into the adsorbate system. In the reverse process of vibrational energy relaxation, this coupling time τ can be interpreted as the vibrational lifetime (T_1) and

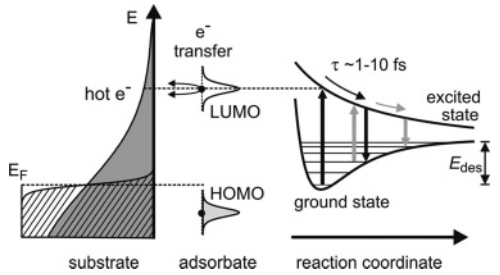

Figure 4. Nonadiabatic energy coupling between electronic and nuclear degrees of freedom. In the DIET/DIMET picture, the electron-mediated energy exchange involves (repeated) transfer of electrons from the high-energy tail of the electronic occupation distribution into an unoccupied molecular orbital of the adsorbate−substrate complex. In contrast, from a cold electron distribution (hatched area), electrons cannot reach the respective unoccupied levels. HOMO and LUMO represent the highest occupied and lowest unoccupied molecular orbitals, respectively. Parts of the figure reproduced from ref 64, Copyright 2002, with permission from World Scientific Publishing Co. Pte. Ltd., Singapore.

correponds to the lifetime contribution to the IR line width of the respective vibration.[9,41] A physical picture of the mechanism of *electronic* friction is given in Figure 2c. Within the Anderson−Newns model,[42] an adsorbate-derived affinity level shifts downward and broadens for decreasing adsorbate−substrate distance. If the level is transiently populated by substrate electrons, the charge-induced adsorbate motion results in a corresponding level shift as the adsorbate starts moving along the corresponding reaction coordinate. Electron flow back and forth between the metal substrate and the adsorbate is intrinsically affected by damping, that is, friction. To which extent adsorbate levels might be populated depends on the electronic temperature of the substrate, as seen in Figure 2c, so usually low-lying energy levels are involved in excitations via electronic friction.

The second substrate−adsorbate coupling scenario accounts only for purely electron-mediated processes and invokes "desorption (or more generally *dynamics*) induced by multiple electronic transitions" (DIMET).[43] In the DIMET process, as illustrated in Figure 4, hot substrate electrons transiently populate a normally unoccupied affinity level, transferring the adsorbate−substrate complex to an electronically excited PES, which can be either antibonding, that is, repulsive, as in the Menzel−Gomer−Redhead[44,45] (MGR) picture or bonding as proposed by Antoniewicz.[46] As an example, Figure 5 displays the results of density functional theory (DFT) calculations for a certain atomic oxygen coverage on ruthenium [O(2 × 1)/Ru]. The oxygen induces the appearance of an antibonding state at such an energy above the Fermi level that the femtosecond-laser-induced hot electron distribution ($T_{el} \approx 6000$ K) can significantly populate this state. The excitation of the O−Ru bond was found to be the crucial and rate-limiting step in the femtochemistry of CO + O on Ru.[17] Similar to the Anderson−Newns model (Figure 2c), the new charge distribution altered by the transient electron transfer in the DIMET picture initiates nuclear motion converting potential energy into kinetic energy. After relaxation back to the electronic ground state, the system has acquired vibrational energy. At high excitation densities, additional excitation/de-excitation cycles might occur before vibrational energy relaxation takes place on the ground-state PES, thus enabling the adsorbate to accumulate sufficient energy in the relevant coordinate to overcome the reaction barrier. Experimentally, a nonlinear dependence of the reaction yield on the absorbed laser fluence is a

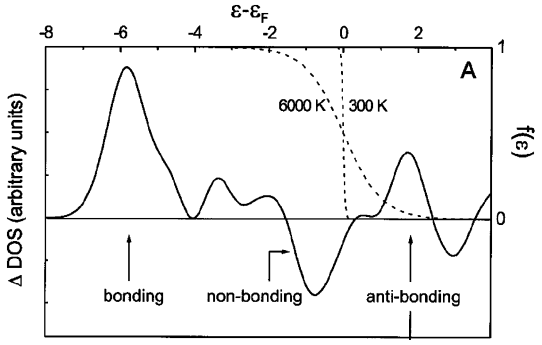

Figure 5. Density of states (DOS) of 0.5 ML of atomic O on Ru(0001) obtained by density functional theory. The solid line displays the difference in the DOS between the O(2 × 1)−Ru(0001) structure and the bare Ru(0001) surface. A bonding state appears well below the Fermi level, here denoted by ϵ_F, and an antibonding state 1.7 eV above ϵ_F. Fermi functions, $f(\epsilon_F)$ (dashed lines, right ordinate axis), for 300 and 6000 K demonstrate that with increasing temperature the antibonding level becomes populated. Reprinted with permission from *Science* (http://www.aaas.org), ref 17. Copyright 1999 American Association for the Advancement of Science.

characteristic consequence of multiple repetition of such excitation/de-excitation cycles.[13,14,43] An adsorbate-mass-dependent reaction yield (also referred to as isotope effect) can also be rationalized in the DIMET picture, in which the lighter reactant will have gained more vibrational energy after relaxation back to the ground state than its heavier counterpart due to the mass-dependent acceleration on the excited potential energy surface.

The two concepts (friction model and DIMET) incorporate similar physical processes in a different mechanistic description. The electronic levels and excitations involved in both scenarios have distinct characteristics: At low excitation densities, in the friction view, low energy levels play the crucial role and high-lying adsorbate resonances will not be reached (see Figures 2c and 4). However, these high-lying resonances are exactly those levels that are populated in the DIMET picture by electrons from the high-energy tail of a hot Fermi−Dirac distribution (or by nonthermalized photoexcited electrons, see Figure 2a). At high excitation densities (i.e., where multiple electronic transitions between the ground and excited state PES occur), both scenarios are physically equivalent, and the DIMET process would correspond to a strongly temperature-dependent electronic friction coefficient in the friction model. A unifying formalism is given in ref 40.

For a quantitative theoretical description of the energy transfer from the laser-excited substrate to the reactants in the adsorbate layer, frictional coupling between the electron and phonon heat bath to a harmonic oscillator of the adsorbate motion is typically used. Based on a master equation formalism,[39,47] the time evolution of the energy content of the adsorbate is represented by[48]

$$\frac{\mathrm{d}}{\mathrm{d}t}U_{ads} = \eta_{el}(U_{el} - U_{ads}) + \eta_{ph}(U_{ph} - U_{ads}) \qquad (4)$$

with the Bose−Einstein distributed mean vibrational energy

$$U_x = \frac{h\nu_{ads}}{\mathrm{e}^{h\nu_{ads}/(k_B T_x)} - 1} \qquad (5)$$

of an oscillator at temperature T_x. ν_{ads} refers to the frequency

of the vibration along the reaction coordinate. In this so-called *empirical* friction model, accounting for both electronic and phononic contributions, the adsorbate temperature, T_{ads}, is obtained by solving eq 4 with T_{el} and T_{ph} computed with the two-temperature model,[12] which was outlined in the previous subsection. The reaction rate, R, and, finally, to compare with the experiment, the reaction yield, Y, as the time integral of R are calculated with an Arrhenius-type expression

$$R = -\frac{d}{dt}\theta = \theta^n k_0 \, e^{-E_a/(k_B T_{ads})} \quad (6)$$

where θ and n denote the coverage and the order of the reactions kinetics, respectively.

As an alternative, a *modified* friction model has been proposed by Brandbyge and co-workers,[40] in which a purely electronic frictional coupling is incorporated. Here, the frictional force originates from coupling of Langevin noise of the electron heat bath (T_{el}) into the adsorbate center of mass coordinate (T_{ads}). Based on the same master equation as in the former case, one obtains the adsorbate temperature, T_{ads}, by solving

$$\frac{d}{dt}T_{ads} = \eta_{el}(T_{el} - T_{ads}) \quad (7)$$

The reaction rate scales proportionally with the desorption probability, which in turn depends similarly as in the empirical model on a Boltzman factor

$$R(t) \propto P_{des}(t) = E_a \int_0^\infty dt \, \frac{\eta_{el}}{T_{ads}} \, e^{-E_a/(k_B T_{ads})} \quad (8)$$

However, in contrast to eq 6, the friction coefficient η_{el}, T_{ads}, and the energy E_a enter the pre-exponential factor. Taking into account the mass dependence of the friction coefficient, $\eta_{el} \propto 1/m$,[49] the Brandbyge model[40] directly leads to an isotope effect in the reaction yield for isotopically substituted reactants, in contrast to the empirical model discussed above. Note that within both frictional models the energy E_a is the well depth of a truncated one-dimensional harmonic oscillator. However, it turns out that values for E_a extracted from experimental data exceed the measured activation energies for desorption (typically by ~30%, see, for instance, ref 38). It has been speculated that either the dynamics on a multidimensional PES is the origin of this discrepancy[50] or that E_a should be regarded as a modified activation energy that is larger than the depth of the adsorption well indicating the population of electronically excited states.[18]

A typical outcome of quantitative modeling of a femtosecond-laser-induced surface reaction is given in Figure 6. Like in Figure 1, bottom panel, the electron temperature rises within few hundreds of femtoseconds to several thousand kelvin and then relaxes due to cooling to the phonon system (phonon temperature not shown here) and heat transport into the bulk. With a short but finite time delay, the adsorbate temperature increases depending on the friction coefficient η_{el}, which is typically assumed to be constant in the low-excitation limit. However, recent experiments on femtosecond-laser-induced oxygen diffusion on a Pt(111) surface[51] indicate that a constant, temperature-independent η_{el} is insufficient to correctly describe the experimental data; details will be given in section 6.1. Moreover, the underlying one dimensionality of the coupling models described so far certainly fall short in reactions with highly complex and multidimensional reaction coordinates.[52,53] Examples of multidimensional friction will be discussed in section 6.1 ("Multidimensional Dynamics").

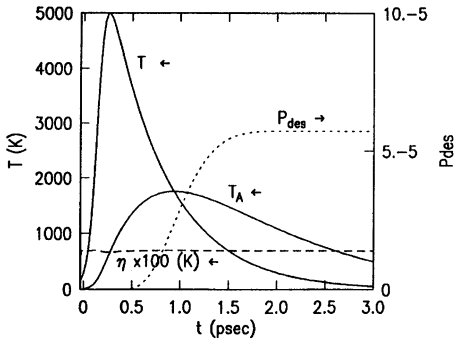

Figure 6. Time dependence of various quantities in a femtosecond-laser-induced desorption reaction driven by electronic friction between substrate electrons and the adsorbate. Typical time profiles are shown for the electronic temperature, $T(t)$, the adsorbate temperature, $T_A(t)$, and the desorption probability, $P_{des}(t)$. The numerical values correspond to the desorption of NO from Pd(111) where the electronic friction coefficient, $\eta(t)$, is nearly constant. Reprinted with permission from *Phys. Rev. B* (http://link.aps.org/abstract/PRB/v52/p6042), ref 40. Copyright 1995 American Physical Society.

3. Experimental Implementation

Surface femtochemistry experiments are performed by applying amplified femtosecond-laser pulses to well-defined metal/adsorbate systems in ultrahigh vacuum (UHV), see Figure 7. While laser fluences up to several 100 J/m^2 (close to the damage threshold of the substrate) are necessary to realize a chemical reaction to a substantial extent, UHV base pressures of typically $<1 \times 10^{-10}$ mbar in conjunction with standard surface science tools are required for preparation and characterization of the substrate and the adsorbed reactants. To obtain information on the various aspects of an ultrafast photoinduced surface reaction, different experimental techniques have to be applied. All of them rely on subpicosecond laser pulses, which trigger the reaction. Subsequently, mass spectrometry, photoionization techniques, or optical methods probe the evolving system response upon laser excitation. As illustrated in Figure 7, top panel, in two-pulse correlation and fluence dependence experiments (details given in respective sections of chaper 5), the reaction yield is detected as a function of the pulse−pulse time separation and the absorbed fluence, respectively. In addition, this yield might depend on the excitation wavelength, the reactants' mass (referred to as isotope effect), and the adsorbate coverage. To identify peculiarities of a femtosecond-laser-induced reaction in comparison to the reaction initiated under thermal equilibrium conditions (if possible), thermal desorption spectroscopy (TDS) is used.

Measurements of the internal energy content (vibrational and rotational) of the desorbing reaction product particles involve in most cases state-selective ionization of these species via resonance-enhanced multiphoton ionization (REMPI). To this end, the femtosecond-laser setup needs to be synchronized to a tunable excitation laser, see Figure 7, bottom panel. Insights obtained from this kind of experiments involve the rovibrational population distributions of the desorbing molecules. Besides energy-partitioning information [together with time-of-flight (TOF) measurements], the state-

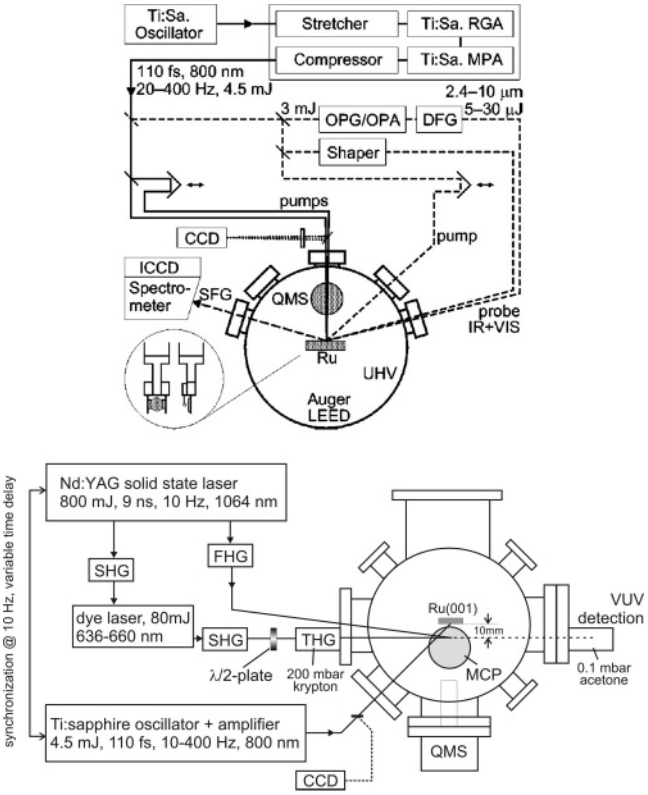

Figure 7. Schematic diagrams of two typical setups for surface femtochemistry experiments. The basic ingredients comprise a high-power femtosecond laser and an ultrahigh vacuum system, in which the sample is prepared and analyzed. (top) Laser-induced desorption experiments with mass spectrometry as analysis technique are performed as indicated by the solid lines of the optical beam path. The dashed lines show the setup for all-optical studies using sum-frequency generation as detection method. Reprinted with permission from ref 37. Copyright 2000 American Institute of Physics. (bottom) For state-selective measurements of the desorbing product particles, the reaction initiating femtosecond laser is synchronized with a tunable detection laser system (here, a VUV source). Reprinted with permission from *Phys. Rev. B* (http://link.aps.org/abstract/PRB/v72/e205404), ref 52. Copyright 2005 American Physical Society.

selective detection scheme enables access to a potential molecular alignment of the reaction product by varying the polarization of the exciting laser pulse.[52,54] Finally, time-resolved optical pump−probe studies exploit an optically induced product-specific system response as a function of the time delay between pump and probe pulse. As also outlined in the top panel of Figure 7, for example, in an experimental setup for surface-sensitive vibrationally resonant sum-frequency generation (SFG), the signal is spectrally dispersed and acts as a probe in such a pump−probe spectroscopy experiment.

Technical details on the various femtosecond laser systems, the UHV chambers including mass spectrometer detection units, and sample preparation procedures can be found in the respective original articles, which are summarized in terms of the investigated adsorbate/substrate system in Table 1.

4. Brief History of Surface Femtochemistry

A long-standing goal in surface science has been the control of surface reactions by light. While such attempts date back many decades,[55] it took until the late 1980s to establish the field of nonthermal surface photochemistry.[56] In experiments with nanosecond-laser (or continuous wave, cw) excitation, various photostimulated processes such as desorption, dissociation, and reactions of molecules adsorbed at metal surfaces were investigated, which showed a *linear* dependence of the reaction yield on the number of absorbed photons by the substrate. These findings could only be rationalized by an underlying excitation mechanism, which invokes a process like desorption induced by (a single) electronic transition (DIET). In 1990, the IBM group of Heinz and co-workers reported a novel nonthermal desorption mechanism for NO/Pd(111) induced by femtosecond laser pulses.[23] These experiments revealed a highly *nonlinear* fluence dependence. Using a two-pulse correlation scheme (details given in section 5.2 "Sequential Excitation"), the IBM group could demonstrate a subpicosecond response time and attribute this process to nonadiabatic coupling of the desorption coordinate to the transient nonequilibrium electron temperature in the metal substrate.[13] In two pioneering papers, the basic theoretical concepts of electron−nuclear coupling via electronic friction[47] and desorption induced by multiple electronic transitions[43] (DIMET) between two diabatic PESs were subsequently developed. This newly established field of surface femtochemistry then attracted increasing attention in the years thereafter.

First, we briefly summarize the development of surface femtochemistry since the first reports of Heinz and co-workers[23] in terms of the various adsorbate−substrate systems and the chemical and physical processes investigated thereby. However, we refrain from a comprehensive discussion of all publications found in the literature that report progress in surface femtochemistry but will highlight the main achievements in this field. Table 1 provides an overview of chemical processes at metal surfaces induced by femtosecond-laser pulses. A significant part of surface femtochemistry has focused on the desorption of diatomic molecules such as NO, CO, or O_2. The dynamics of this process can be treated in a simplified model using a single active degree of freedom, namely, the center of mass coordinate. We will discuss the prototype systems NO/Pd(111) and O_2/Pt(111) in more detail in section 5. A second important class of processes invokes femtochemical reactions between coadsorbed atomic or molecular reactants (see Table 1). Such processes are expected to invoke multidimensional reaction dynamics. Pioneered by Ho and co-workers[15] and later on by Mazur and co-workers,[34] the CO oxidation reaction ($^1/_2O_2 + CO \rightarrow CO_2$) on Pt(111) has served as a prototype of this kind of molecular formation/association reactions. In such a formation reaction of CO_2 on platinum, transiently formed atomic oxygen (resulting from the dissociation of molecular oxygen) reacts with coadsorbed CO similar to the reaction under thermal (equilibrium) conditions. In contrast, in the case of CO oxidation on Ru(0001), Ertl and co-workers[17] could show for the first time that hot electron-mediated activation of coadsorbed atomic oxygen can induce a chemical reaction that is not accessible under equilibrium conditions. This means that the reaction path for CO oxidation on Ru is "switched on" only by femtosecond-laser excitation. During the past few years, the associative formation and desorption of molecular hydrogen ($H + H \rightarrow H_2$) on Ru by excitation of the chemisorbed atomic species (H, D) has also been demonstrated.[18,38,52,57] This elementary reaction belongs to the most extensively studied systems in surface femtochemistry and will be discussed in detail in

Table 1. Overview of Surface Reactions Induced by Femtosecond Laser Pulses

system	process	measurements[a,b]	peculiarities[b]	refs
NO/Pd(111)	desorption	yield-FD, 2PC, TOF, E_{vib}, E_{rot}		13, 23, 39
NO/Pt(111)	desorption	2PC, TOF, E_{rot}	final-state-dependent measurements	66
O_2/Pt(111)	desorption	yield-FD, 2PC, TOF, wavelength, σ_{rx}	nonthermalized e^-	16, 34, 65, 67, 68, 181
O_2/Pd(111)	desorption	yield-FD, 2PC, isotope	desorption/dissociation branching ratio	14, 69, 182
CO/Pt(111)	desorption	yield-FD, 2PC, wavelength, IR pump−SFG probe	nonthermalized e^-	34, 71
CO/Cu(100)	desorption	yield-FD, 2PC, E_{vib}, E_{rot}, TOF		48
CO/O_2/Pt(111)	CO + O association	yield-FD, TOF, wavelength		15, 16, 67, 68
O_2/C_2H_4/Pt(111)	CO, CO_2, H_2O formation	TOF		183
C_6H_6/Pt(111)	desorption	TOF		184, 185
CO/Ru(001)	desorption	yield-FD, 2PC, IR pump−SFG probe		17, 37, 60
CO/O/Ru(001)	CO + O association	yield-FD, 2PC, isotope	therm. inaccessible	17
H/Ru(001)	H + H association	yield-FD, 2PC, isotope, TOF, E_{vib}, E_{rot}, $A_0^{(2)}$, coverage, σ_{rx}		18, 38, 52, 57
H/O/Ru(001)	2H + O association	TOF	therm. inaccessible	64
C/O/Ru(001)	C + O association	yield-FD, 2PC, isotope, TOF		85
O/Pt(111)	diffusion	hopping rate FD, 2PC	SHG probe	51, 74
CO/Cu(110)	diffusion		STM analysis, not real time	58
CO/Pt(111)	restructuring		SFG analysis, not real time	186
CO/Cu(111)	desorption	vis pump−SHG probe		128
CO/Pt(533)	diffusion	IR pump−SFG probe		59

[a] Measurements include fluence dependence of the reaction yield (yield-FD), two-pulse correlation (2PC) experiments, isotope effects (isotope), time-of-flight distributions (TOF), state-selective detection of the internal energy content (E_{vib}, E_{rot}), molecular alignment studies ($A_0^{(2)}$), and coverage- and wavelength-dependent reaction yield and reaction cross sections (σ_{rx}). [b] Further experimental techniques that provide additional information are second-harmonic (SHG) and sum-frequency (SFG) generation, as well as scanning tunneling microscopy (STM).

sections 5 and 6. Very recently, a new class of femtochemical processes, namely, femtosecond-laser-induced diffusion, has been reported. In these experiments, nonadiabatic coupling of substrate electrons to nuclear degrees of freedom induces translational (lateral) motion of the adsorbate (see Table 1). Pioneering studies have been performed for CO on various substrates and O on platinum, whereby the diffusion process was probed by scanning tunneling microscopy[58] and nonlinear optics.[51,59]

Finally, we like to highlight the main experimental and theoretical achievements that have helped the field to significantly advance a deeper and more reliable and quantitative understanding of chemical reaction dynamics in surface femtochemistry; details will be outlined further in the subsequent sections. Stephenson and co-workers introduced the concept of a yield-weighted fluence to account for the highly nonlinear dependence of the reaction yield on the spatial profile of the laser pulses.[48] In desorption experiments, this procedure is a prerequisite for a quantitative comparison between the measured reaction yield and model calculations. Isotope substitution experiments have been successfully used to obtain additional insights into the excitation mechanism,[18,38] the adsorbate−adsorbate interactions,[18,38,57] and the rate-limiting step in bimolecular reactions.[17] However, the most detailed information can be obtained by state-resolved detection of desorbing reaction products. The energy partitioning into the rotational, vibrational, and translational degrees of freedom provides a critical benchmark for microscopic theories. Prototypical studies along these lines have been performed for the CO desorption from Cu(001)[48] and the associative D_2 formation on Ru(0001).[52,53] A further promising development is the application of time-resolved nonlinear optical spectroscopy (in particular vibrational sum-frequency generation) to probe the elementary processes at the surface directly in real time via the optical response en route along the reactants' trajectory. This approach has been successfully used for CO desorption from ruthenium[60] and CO diffusion on stepped platinum.[59] On the theoretical side, one of the main achievements was the formulation of the (one-dimensional) electronic friction model by Brandbyge et al.[40] and its connection to the DIMET picture for surface femtochemistry. Based on the earlier concept of multidimensional molecular dynamics with electronic frictions by Head-Gordon and Tully,[61,62] the traditionally one-dimensional electronic friction model has been very recently extended to inherently multidimensional systems such as association reactions. Here, ab initio calculations of the friction coefficients and the PES allow a complete simulation of the nonadiabatic reaction dynamics under the influence of electronic friction.[53,63] The application of these multidimensional friction calculations to the H_2/Ru(001) system will be discussed in detail in section 6.1.

5. Experimental Observables and Implications on Reaction Dynamics

This section is to explain the different classes of experimental approaches that measure the relevant observables of a femtosecond-laser-induced surface process. In the majority of the experiments,[13−18,23,34,37−39,48,52,57,64−69] the reaction yield is detected by mass spectrometry as a function of various experimental parameters such as (i) the absorbed laser fluence, (ii) the time profiles of laser excitation, for example, pulse sequences or varying pulse duration, (iii) the photon energy of the exciting laser pulse, (iv) the mass of the reactants reflecting isotope effects, and (v) the structure of the adsorbate−substrate system. Unlike these cases, where the mere occurrence of the reaction product at the detector (mass spectrometer) is sufficient, a second class of approaches focuses on the photoproduct itself to obtain detailed information on the internal energy content.[23,48,52,66] Here, either the ionization yield or the laser-induced fluorescence

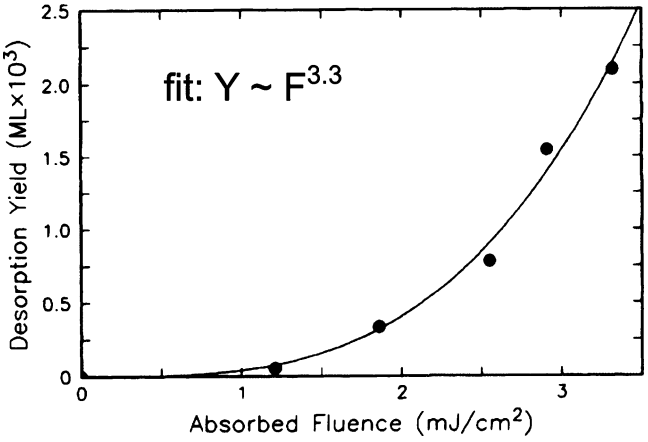

Figure 8. NO desorption yield from Pd(111) in monolayers as a function of the absorbed laser fluence with 620-nm 200-fs laser pulses. The solid line represents a fit to a power law F^n with exponent $n = 3.3$. Note that in these early pioneering measurements, no yield-weighting procedure (see text) as established first in ref 48 was applied. Instead, the fluence was measured here in a broad region of the maximal intensity of the laser beam. Reprinted with permission from *Phys. Rev. Lett.* (http://link.aps.org/abstract/PRL/v64/p1537), ref 23. Copyright 1990 American Physical Society.

of the desorbing particles is measured. The information on the reaction dynamics, however, derived from all these experiments mentioned so far is indirect in the sense that the experimental observables are taken long after the actual ultrafast reaction process is complete. Complementary information can be obtained in real-time studies, where the optical properties of the adsorbate-covered surface are probed in-situ under transient conditions. To this end, typical all-optical pump−probe techniques apply nonlinear spectroscopy methods such as SFG.[59,60,70,71] Finally, very few examples can be found where the photoemission of an adsorbate−substrate system undergoing a chemical reaction is detected by two-photon photoemission (2PPE) spectroscopy[72] or ultraviolet or X-ray photoelectron spectroscopy (UPS or XPS, respectively).[73] Again, these approaches allow only indirect access to the underlying reaction dynamics.

In the following, we will discuss the different experimental observables for exemplary adsorbate−substrate systems. In the case of desorption of *molecular* species, we will focus on the NO/Pd(111) and O_2/Pt(111) systems. In reactions where *interatomic chemical bonds* are formed, we concentrate on the recombinative $H + H \rightarrow H_2$ desorption and the CO oxidation, $CO + O \rightarrow CO_2$, both on the Ru(001) surface. Exceptional results of other systems and new and only infrequently applied experimental approaches will also be mentioned.

5.1. Fluence Dependence of Reaction Yield

Femtosecond-laser excitation of an adsorbate-covered metal substrate results in a distinctive relationship between the reaction yield and the absorbed laser fluence. As one of the first examples, Prybyla et al.[23] showed the nonlinear desorption yield of NO from a Pd(111) surface as a function of the absorbed laser fluence, see Figure 8. Such a strong nonlinearity of the yield with increasing laser fluence is a characteristic of a femtosecond-laser-initiated surface process (in contrast to the linear dependence observed in cw- or nanosecond-laser-induced photochemistry mediated by substrate electrons[56]). Typically, the experimentally observed yield-vs-fluence ($Y-F$) dependence is parametrized by a power law of the form $Y = F^n$ with exponents n ranging from 3 to 8. An exceptionally high value of $n = 15$ was obtained in femtosecond-laser-induced diffusion of atomic O on Pt(111) by Stépán et al.[74] Yet in all cases, the power-law relation is introduced only empirically in order to quantify the observed fluence dependence with a single number, and it should be noted that this representation might be valid only in a limited fluence range. When saturation effects come into play, a clear deviation from such a uniform power-law behavior is found as manifested in a leveling-off in the reaction yield with increasing laser fluences and demonstrated, for instance, in the highly efficient recombinative desorption of hydrogen from Ru(001).[18]

This nonlinearity of the reaction yield as a function of laser fluence, however, has certain consequences. First, the overall process cannot be described by a single and fixed quantum efficiency, which means that the reaction cross section σ needs to be specified with a particular laser fluence. A typical σ for photon-induced desorption of neutrals from metal surfaces lies between 10^{-18} and 10^{-20} cm^2.[75] In surface femtochemistry, the already mentioned $H + H \rightarrow H_2$ recombinative desorption from Ru(001) exhibits one of the most efficient photoreactions with values of $\sigma = 7 \times 10^{-18}$ cm^2 at $F = 60$ J/m^2 and as high as 10^{-17} cm^2 for $F > 100$ J/m^2.[18] Second and most importantly, it is essential to account for the spatially nonuniform energy distribution across the laser beam profile. Thereby, each section of the beam profile contributes to the overall reaction yield according to its fluence in a nonlinear manner. The pulse energy and spatial profile of the laser beam have to be recorded for each measurement at a particular laser fluence, and the experimental tools therefore have to be included in the setup as shown in Figure 7, top panel. A yield-weighting procedure[48] is usually applied in which each beam profile fraction is weighted with its respective yield resulting in the absorbed yield-weighted fluence $\langle F \rangle$; by parametrization of the fluence dependence of the desorption yield Y with a power law $Y \propto \langle F \rangle^n$, $\langle F \rangle$ is obtained by summing over the entire laser beam profile (represented by the CCD camera pixels of the beam profiler in the optical reference channel, see Figure 7) according to $\langle F \rangle = \sum Y_i F_i / \sum Y_i = \sum F_i^{n+1} / \sum F_i^n$. Here n is a parameter of a self-consistent fit to the experimental data set. It should be noted that this accounting for the nonuniformity of the excitation beam profile by yield-weighting should be applied as a standard if the desorbing particles are probed; see, for instance, refs 18, 37, and 48. In contrast, for optical probe techniques, this procedure might not be necessary if a probe spot size is used that is is sufficiently smaller than the excited area on the sample (e.g., see ref 50).

The DIMET concept (see section 2.2. "Substrate−Adsorbate Coupling") of *multiple* electronic transitions in the substrate−adsorbate complex helps to understand the origin of the experimentally observed nonlinearity of the reaction yield fluence dependence. In the DIET limit, a *linear* yield versus fluence relation should prevail. Note, however, that a value $n > 1$ for the power-law exponent does not represent the exact number of excitation−de-excitation cycles in a DIMET process needed to overcome the reaction barrier or leave the adsorption well, see Figure 4. Moreover, the observation of a nonlinear fluence dependence of the reaction yield does not allow one to draw conclusions regarding the excitation mechanism via substrate electrons or phonons (see section 2.2). A nonlinear $Y-F$ dependence is indeed con-

sistent with a hot electron-mediated reaction mechanism but does not exclude a phonon-driven scenario due to the nonlinearity of the Arrhenius factor governing a thermally activated process. For example, the (predominantly) phonon-mediated femtosecond-laser-initiated CO desorption from Ru(001) also exhibits a strongly nonlinear yield as a function of the absorbed fluence, $\langle F \rangle$, with $n = 4.5$.[37] Consequently, other measurements are necessary to unambiguously distinguish among the different pathways of energy flow from the metal substrate to the reactants in the adsorbate layer, as will be described in the following two sections.

5.2. Sequential Excitations: Two-Pulse Correlation, Variation of Pulse Width, and Chirp

As mentioned in section 2.2. ("Substrate−Adsorbate Coupling"), in a substrate-mediated surface reaction, each of the substrate's subsystems, electrons and phonons, can couple to reactants in the adsorbate layer independently. A direct way to differentiate between such electron- and phonon-mediated reaction pathways and to obtain insights into the dynamics of the underlying excitation mechanism is provided by so-called two-pulse correlation (2PC) measurements with a time resolution only limited by the laser pulse duration: Two cross-polarized pulses of nearly equal intensity are sent onto the adsorbate-covered surface, and in most cases, the time-integrated reaction yield is measured with a mass spectrometer as a function of the pulse−pulse delay.[76] Due to the typical nonlinear dependence of the reaction rate on the incident laser fluence (see section 5.1), the width of the resulting yield correlation function critically depends on the excitation pathway. A narrow full width at half-maximum (fwhm) of only a few picoseconds is a clear indication for the operation of the hot electron, that is, DIMET-like reaction mechanism, since only for pulse separations shorter than the electron−phonon equilibration time, the electron temperature is greatly enhanced due to the combined effect of both excitation pulses. In contrast, a phonon-mediated process proceeds on a much slower time scale of tens of picoseconds due to the significantly longer energy storage time within the phonons compared with the electronic system and the slower coupling time from the phonon bath into the reaction coordinate. Note that energy can also be stored in low-energy vibrational modes of the adsorbate on the time scale of vibrational energy relaxation. The latter may be comparable to the cooling time of the substrate phonons (~10 ps), and for a vibrationally assisted desorption process, the 2PC trace would then exhibit wings on a corresponding time scale.[14] Finally, it should be mentioned that a reaction initiated by *direct* absorption of the exciting laser pulse should feature a two-pulse yield correlation width on the order of the pulse duration.

Figure 9 illustrates how the excitation by a two-pulse sequence leads to the described features of the yield correlation function. Calculated with the 2T model (see section 2.1), for an exemplary pulse−pulse delay of $\Delta t = 5$ ps, the metal substrate (here ruthenium) is excited by two femtosecond pulses, leading to an electronic and phononic temperature time profile similar to Figure 1, however, with the second pulse striking the surface while both subsystems are still at elevated temperatures. If one now plots the maximum temperature T_{el}^{max} and T_{ph}^{max} reached in the electron and the phonon heat bath as a function of Δt, a narrow and a broad maximum temperature distribution is obtained, respectively. For $T_{el}^{max}(\Delta t)$, this is rationalized by the sharp

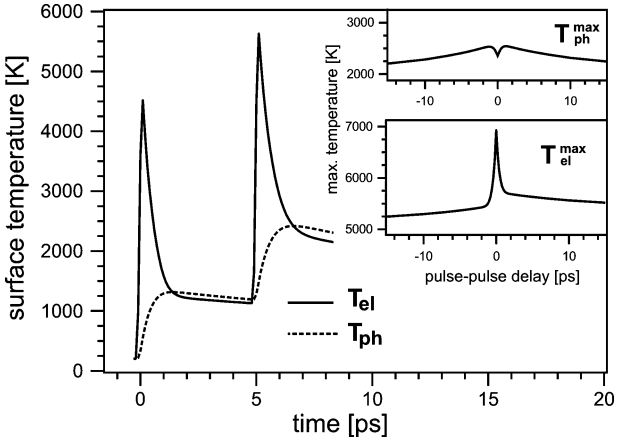

Figure 9. Surface temperature transients of the electron and phonon system, T_{el} and T_{ph}, respectively, for ruthenium after excitation with a pair of two 800-nm, 110-fs pulses with 120 J/m^2 absorbed fluence each and a temporal pulse−pulse separation of exemplary 5 ps. Calculations are performed based on the two-temperature model (see eqs 1 and 2). The inset displays the overall peak electron and phonon temperatures, T_{el}^{max} and T_{ph}^{max}, as a function of the pulse−pulse delay. Note the resulting narrow and broad distributions for T_{el}^{max} and T_{ph}^{max} with a fwhm of only a few picoseconds and several tens of picoseconds, respectively. Reproduced with permission from ref 37. Copyright 2000 American Institute of Physics.

rise and fall of the electronic temperature transient $T_{el}(t)$, while the phonon temperature cools significantly more slowly. Consequently, due to the nonlinear relation between T_{el} and T_{ph}, respectively, and the adsorbate temperature, T_{ads} (see eqs 4 and 7), the two-pulse correlation of the reaction rate R and hence the yield as the time integral of R reflects the respective width of these peak temperature distributions (see eqs 6 and 8). Before discussing different experimental 2PC measurements, it should be noted that the T_{ph}^{max} function exhibits a clear temperature decrease at zero time delay (see inset of Figure 9); this dip is caused by the competition between electron−phonon coupling and the hot-electron heat transfer away from the surface. As seen from eqs 1 and 2, the T_{el} dependence of these processes is different, resulting in a stronger energy loss at the surface of the substrate at higher electronic temperatures due to the increased heat transport into the bulk.[37] How this theoretical prediction in the framework of the 2TM is manifested experimentally will be demonstrated further below. Second, the apparent asymmetry in the electronic maximum temperature trace is caused by the experimental (usually inevitable) small deviation from perfectly equal beam intensities of the two pulses. It should be mentioned, however, that slightly asymmetric intensities of both pump pulses are even advantageous for practical reasons in the data analysis. In this case, the fitting of a 2PC trace in electronic friction calculations is very sensitive with respect to the activation energy, E_a, and the coupling time, $\tau_{el} = 1/\eta_{el}$.

Figure 10 shows two-pulse correlation measurements by Bonn et al.[17] for the femtosecond-laser-induced desorption of molecular CO and the CO + O → CO_2 oxidation from the O/CO coadsorbate system on Ru(001). The fwhm of the correlation function for both processes are significantly different. While the CO desorption exhibits a width in the 2PC of 20 ps, the CO oxidation shows a much faster response with a 2PC fwhm about one order of magnitude narrower in the few picosecond range (3 ps). Accordingly, the CO desorption process was attributed to be phonon-mediated, contrary to the oxidation of CO, which is clearly driven by

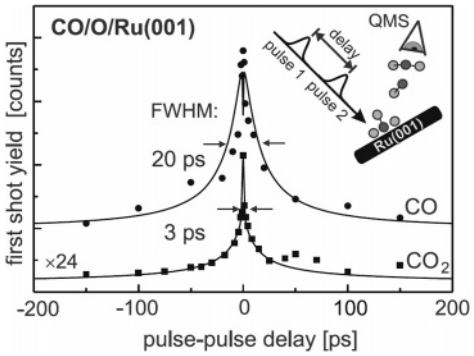

Figure 10. Two-pulse correlation measurements of the femtosecond-laser-induced CO oxidation yielding CO_2 (squares) and the CO desorption (circles).[17] Yields are scaled and offset. Solid lines are obtained using appropriate friction models (refs 40 and 39). The data for the hot-electron-mediated CO_2 formation is reproduced best with fit parameters $E_a = 1.8$ eV as activation energy and $\tau_{el} = 0.5$ ps for the electronic friction coupling time. The principle of the two-pulse correlation technique is shown as inset. Reprinted with permission from ref 187. Copyright 2000 Springer-Verlag.

hot substrate electrons. Both sets of experimental correlation data together with their respective yield-vs-fluence dependence measurements are well reproduced by friction model calculations, also shown in Figure 10. As outlined in section 2.2., the coupling times, τ_{el} or τ_{ph}, and the activation energy, E_a, are taken as fit parameters in such modeling. The value of $E_a = 1.8$ eV obtained from the modified electronic friction model (eq 8) in the case of CO + O → CO_2 is in nice agreement with DFT calculations for the electronic structure of atomic oxygen [O(2 × 1)] on Ru(001).[17] At 1.7 eV above the Fermi energy, an antibonding state appears (Figure 5), which—in the DIMET picture—is transiently populated by hot substrate electrons. The activation of the O−Ru bond appears to be the rate-limiting step. All these findings corroborate the electronic nature of the excitation process in the femtosecond-laser-induced CO oxidation on Ru(001).

By contrast, the femtosecond-laser-induced desorption of CO molecules from Ru(001) is well understood as a phonon-driven reaction (no electronic contribution, that is, $\tau_{el} = \infty$). The empirical friction model (eq 6) provides good fits to the two-pulse correlation and yield-vs-fluence data with a phonon-coupling time of $\tau_{ph} = 1$ ps and activation energies E_a of 1.2 and 1.65 eV, respectively, depending on the initial CO coverage.[37] However, also purely electronic excitation scenarios (finite $\tau_{el} \approx 2$ ps and infinite τ_{ph}) can lead to moderate agreement with the CO desorption data from Ru(001). The reason for this is that the outcome of the frictional calculations with these parameters is almost identical to the case of the purely phonon-mediated reaction described above. This ambiguity is inherent to the frictional model used since for electronic coupling times, τ_{el}, longer than the electron−phonon equilibration time, τ_{el-ph}, the adsorbate temperature, T_{ads}, follows T_{ph}.[37,77] Therefore additional arguments are necessary to decide on either reaction mechanism, phonon or electron mediation. While the electronic structure of the adsorbate−substrate system favors a predominantly phonon-mediated scenario (the CO $2\pi^*$ level responsible for electronic interaction with substrate electrons is not sufficiently populated in the reported experiments to play a major role in the reaction mechanism[78]), recent time-resolved SFG experiments also support some electronic contribution to the CO desorption mechanism.[79] The latter involve measurements of the transient red shift of the C−O stretch vibration during CO desorption. It is found that this C−O frequency shift due to anharmonic coupling of the internal C−O mode to external motions such as the frustrated translation and rotation sets in *instantaneously* without time delay when the Ru(001) substrate is excited by the desorption triggering pump pulse. Details on these kinds of experiments will be given in section 5.7, "Real-Time Studies".

As noticeable in Figure 10, the calculated 2PC of the CO desorption yield exhibits a substantial dip at zero time delay. It originates as mentioned earlier from the more efficient heat transport of hot electrons into the bulk vs energy transfer into the phonon system via electron−phonon coupling. Due to the nonlinearity of the diffusion term, $\nabla_z(\kappa(T_{el})\nabla_z T_{el})$, in eq 1 with respect to T_{el}, higher electronic temperatures cause a decrease of the maximum phonon temperature at the surface. Thus, the dip in the maximum phonon temperature, T_{ph}^{max}, reflects the spike in the electronic temperature distribution, T_{el}^{max}, of Figure 9. This effect was ignored in early experiments on the CO desorption from Cu(100) by Struck et al.[48] The dip in the phonon temperature and consequently in the desorption yield was then pointed out by Funk et al. in their work on CO on Ru(001).[37] However, the authors found this dip only theoretically in friction model calculations (see Figure 11, top panel). Yet their experimental data of the CO desorption are indeed consistent with the calculated 2PC trace within the error bars of the experiment but did not directly indicate the decrease of the CO yield at zero delay. Similar results in experiment and model could be shown by Denzler et al.[38] in the associative desorption of D + D → D_2 also from Ru(001).

However, the validation of the dip prediction by the 2TM calculations could be achieved by three-pulse transient reflectivity measurements (pump−pump/reflectivity probe) on various metals.[80] Figure 11, bottom panel, demonstrates that for Au, Cu, Cr, and Ru, the reflectivity drops between 5% and 10% if both pump pulses coincide (see Figure 9). With decreasing electron−phonon coupling strength, the reflectivity dip around zero delay becomes deeper but also wider. For desorption experiments, it should be noted that the dip in the calculated yield is more pronounced compared with that in the phonon temperature due to the Arrhenius-type desorption dynamics, where T_{ads} enters the exponent. The reason that this dip in the reaction yield has not yet been observed experimentally lies in the case of experiments on Ru in the strong electron−phonon coupling and hence a rather narrow yield decrease as a function of the pulse−pulse delay. Thus, for Ru, the typical data scattering in a 2PC measurement exceeds the expected yield decrease at $\Delta t = 0$ ps. However if at all, such a dip should be discernible in experiments on metals with weaker electron−phonon coupling like Cu. Yet, Struck et al.[48] could not observe such a behavior in the femtosecond-laser-induced CO desorption from Cu(100). It appears that either the role of electrons in the desorption process was underestimated or nonequilibrium effects (e.g., consequences resulting from nonthermal electrons, see section 5.4, "Wavelength-Dependent Excitation"), which are not accounted for in the standard 2TM, play a non-negligible role in this particular system.[80]

As an alternative to 2PC measurements to extract information on the mechanism of a surface reaction, the reaction yield can also be measured as a function of the pulse duration. Cai et al.[81] found in desorption experiments of CO from Pt(111) with varying pulse duration from 125 fs to 1.5 ps that by changing the pulse width only from 125 to 250 fs under otherwise identical parameters, the desorption yield

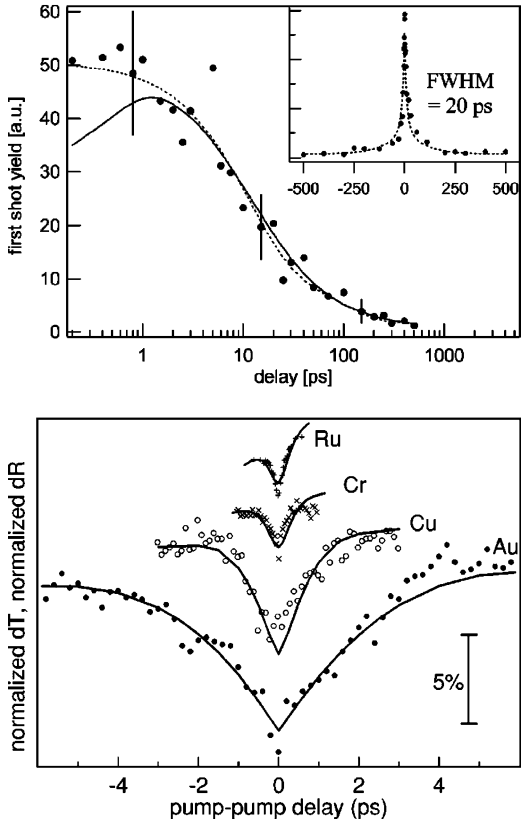

Figure 11. (top) Two-pulse correlation of CO desorbing from Ru(001) indicating a time response of 20 ps fwhm. The dashed lines are a guide to the eye; the solid line represents the outcome of empirical friction-model calculations[39] (see section 2.2). Note that the model predicts a decrease (dip) in the desorption yield at zero delay, which is not discernible in the experimental data within the error margins. Reprinted with permission from ref 37. Copyright 2000 American Institute of Physics. (bottom) Reflectivity changes of various metals as a function of the time delay between two excitation pulses. The experiment involves a double pump-reflectivity probe scheme at a fixed probe delay (several tens of picoseconds). Data sets for Au (700 nm film), Cu (bulk [100] crystal), Cr (200 nm film), and Ru (bulk [001] crystal) are offset for clarity. Lines result from simulations based on the two-temperature model (see section 2.1). Details of the experiment and the modeling are given in ref 80. Note the pronounced dip for all metals at zero delay with decreasing width as the electron−phonon coupling strength increases (coupling constant $g^{Ru} \approx 80g^{Au}$). Reprinted with permission from *Phys. Rev. B* (http://link.aps.org/abstract/PRB/v61/p1101), ref 80. Copyright 2000 American Physical Society.

drops by almost one order of magnitude. Qualitatively, the authors inferred from this pulse width influence and from the strongly nonlinear yield-vs-fluence dependence that frictional coupling of hot-substrate electrons to the adsorbate motion is the dominant reaction mechanism for this system. In the 2TM, the maximum electronic temperature reached at a certain laser fluence strongly depends on the pulse duration, which explains the observed variation in the yield. Although not explicitly performed in ref 81, the standard modeling based on the 2TM in conjunction with electronic friction should in principle reproduce their results.

In addition, in the same experimental study, Cai et al. [81] attempted to experimentally reproduce the predictions by Micha and Yi on the impact of chirped laser pulses on the reaction yield.[82] Based on density matrix theory calculations with the DIMET mechanism inherent in the model, both positive and negative chirp were found to either significantly suppress or enhance the desorption yield of CO from Cu(001). In the experiments on Pt(111), however, no such chirp-induced effect could be unambiguously observed, which was explained by the rather small chirp applied in the experiment and the relatively large scattering of the data.[81] Apart from the demanding task to disentangle the rather complex information obtainable from this kind of experiments with chirped laser pulses, these studies suggest the possibility of optically controlling a surface reaction. The challenges one faces pursuing this goal will be covered in more detail in section 6.3.

5.3. Isotope Effects

Isotope effects are the second experimental observable of a surface reaction, which undoubtedly indicates the operation of an electron-driven mechanism. Unlike in a phonon-mediated process,[83] a ratio of the reaction yield between isotopically substituted reactants different from unity is characteristic for a process involving electronic excitations, for example, in electron-stimulated desorption[84] as well as in surface femtochemistry. As outlined in section 2.2 illustrating the DIMET excitation mechanism, isotope effects are attributed to the mass-dependent acceleration and hence the distance that the isotope travels on the electronically excited PES during its short lifetime (typically a few femtoseconds, see ref 43). Figure 12, top panel, illustrates the origin of the isotope effect in the femtosecond-laser-induced associative desorption of H_2 and D_2 from Ru(001)[38] from the perspective of the frictional description of a femtochemical reaction. According to the Brandbyge[40] model of electronic friction, the electronic coupling time, τ_{el}, is the inverse of the frictional coefficient, η_{el}, and thus scales linearly with the adsorbate mass. Consequently, the lighter reactant gains vibrational energy faster than the heavier counterpart. As depicted in Figure 12, the transient adsorbate temperature, $T_{ads}(H)$, of a H layer rises earlier and reaches higher values than $T_{ads}(D)$ does for a D layer. The slower coupling time for the heavier D atoms is responsible for the fact that the electronic temperature, T_{el}, has already passed its maximum when the D layer starts being excited. Due to the nonlinear dependence of the reaction rate on the adsorbate temperature, the difference in the desorption yields between both isotopes is even enhanced. This applies in particular to the H_2 vs D_2 recombination reaction with the largest possible mass ratio (Figure 12). Indeed for this system, one of the highest values for an isotope effect in surface femtochemistry was reported by Denzler et al.[38] with $Y(H_2)/Y(D_2) \approx 10$ at $\langle F \rangle = 60$ J/m^2. This finding together with a narrow 2PC led to the unambiguous conclusion of an electron-mediated reaction mechanism in the hydrogen desorption from Ru. In addition, in ref 18, Denzler et al. showed for the first time that this isotope yield ratio crucially depends on the absorbed laser fluence. As seen in the bottom panel of Figure 12, both the experimental results and the theoretical modeling based on Brandbyge's friction description exhibit a substantial variation of the $Y(H_2)/Y(D_2)$ ratio as a function of the laser fluence. While for low fluences ($\langle F \rangle \leq 50$ J/m^2) remarkable values for $Y(H_2)/Y(D_2)$ of greater than 20 were observed, this ratio decreases with increasing fluence and is expected to asymptotically approach unity for $\langle F \rangle \rightarrow \infty$. This is because with further increasing electron temperature complete saturation in the photoreaction for both isotopes occurs, that is, desorption probabilities approaching $P_{des}(H_2) = P_{des}(D_2) = 1$.

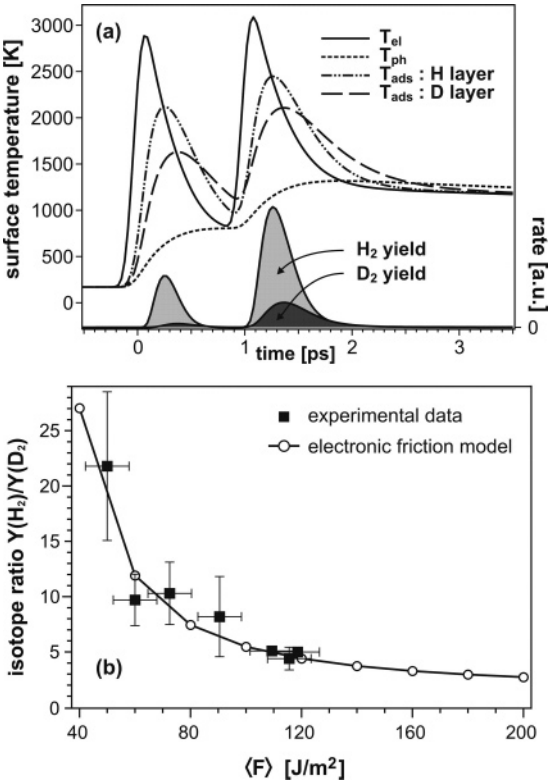

Figure 12. Femtosecond-laser-induced recombinative desorption of hydrogen from Ru(001). (top) Calculated temperature transients caused by two pump pulses (130 fs, 60 J/m^2, 800 nm, 1 ps pulse−pulse separation) for the electron and phonon system of the Ru substrate (obtained from the two-temperature model, ref 12) and the adsorbate temperatures for a H and D layer, respectively (obtained from the modified electronic friction model, ref 40), together with the reaction rate for both H_2 and D_2 recombination. The faster coupling time (i.e., larger electronic coupling) for the lighter isotope results in a higher adsorbate temperature, which in turn leads to a significantly higher reaction yield with respect to the heavier D reactants. Reprinted with permission from *Phys. Rev. Lett.* (http://link.aps.org/abstract/PRL/v91/e226102), ref 38. Copyright 2003 American Physical Society. (bottom) Yield ratio of the H_2 and D_2 recombination as a function of the adsorbed yield-weighted fluence, $\langle F \rangle$. Note that the experimental data are well reproduced by frictional calculations represented by connected open circles. Reprinted with permission from ref 18. Copyright 2004 American Chemical Society.

Besides confirming that a particular surface process is electron-mediated, measurements of the isotope effect also offer the opportunity to determine the rate-limiting step in a multidimensional association reaction (as compared with the less complex desorption process of a diatomic adsorbate). In the femtosecond-laser-induced oxidation experiments of CO + O on Ru(001) by Bonn et al.,[17] a distinct isotope effect from an $^{16}O/^{18}O/CO$ coadsorbate system was found. Here, the authors determined an oxidation yield ratio of $Y(^{16}OCO)/Y(^{18}OCO) \approx 2.2$, while the isotope substitution of the CO reactant did not yield an isotope ratio significantly different from unity. These findings clearly demonstrated that the activation of the Ru−O bond is rate-determining in the CO oxidation reaction on Ru. Finally, it should be noted that in reverse the absence of an isotope effect in the experiment is *not* a sufficient indication that the reaction under investigation *has* to be driven by substrate phonons. In particular, the changes of the reduced mass experimentally accessible might be too small to exceed the scatter of experimental data.

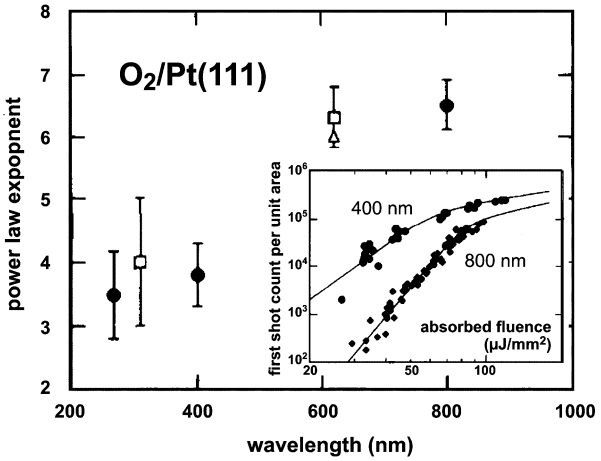

Figure 13. Femtosecond-laser-induced O_2 desorption from Pt(111) and Pd(111), respectively, showing a wavelength dependence of the power law exponent *n* in the parametrization of the nonlinear yield-vs-fluence relation (see section 5.1 and Figure 8). Data points shown here stem from ref 34 (filled circles), refs 15 and 65 (open squares), and ref 14 (open triangle). The inset shows the fluence dependence of the first-shot O_2 desorption yield exemplarily for 400 and 800 nm excitation. Adapted from ref 34, Copyright 1995, with permission from Elsevier.

5.4. Wavelength-Dependent Excitation

Direct optical excitation of the adsorbate, if not negligible, will cause a photon energy dependence of the reaction yield as in gas-phase photochemistry. However, for a substrate-mediated excitation mechanism, which is mostly operative at surfaces, femtochemistry is usually assumed to be induced by a hot but *thermalized* electron distribution. The reaction yield will thus depend solely on the absorbed laser fluence *irrespective* of the photon energy used for excitation (see Figure 2b). If, in contrast, in the DIMET picture a reaction is substantially enhanced due to population of a certain higher lying adsorbate resonance, a distinct wavelength dependence should be observed. Then, nonthermalized energetic electrons in resonance with the adsorbate level may play a significant role in the excitation process. Only a pump pulse of sufficient photon energy can induce transitions to the excited-state PES relevant to the reaction (see Figure 4).

Deliwala et al.[34] showed in experiments on O_2/CO/Pt(111) that both the desorption of O_2 molecules and the CO_2 formation exhibit a pronounced dependence on the excitation wavelength. As shown in Figure 13, the power-law exponent of the yield-vs-fluence relation in the O_2 desorption almost doubles when the wavelength of the exciting laser is changed from the third harmonic at 266 nm to the fundamental at 800 nm. These results strongly suggest that resonant transitions of electrons that are not yet thermalized significantly contribute and favor the O_2 desorption from Pt(111). A similar trend in changes of the fluence nonlinearity of the reaction yield as a function of the excitation wavelength was reported by Kao et al.[15] for the same adsorbate−substrate system. In addition, also for O_2/Pt(111), Busch et al.[68] found a significant wavelength dependence of the O_2 photoyield even in the low-fluence regime in which single electronic excitations are believed to dominate the desorption process.

Since electron equilibration times can be as long as several hundreds of femtoseconds,[31,32] one may ask why nonthermalized electrons do not play a significant role in *all* femtosecond-laser-induced surface reactions. Explanations for this could be (i) the absence of any adsorbate-induced

(long-lived) resonances that are relevant to the reaction and lie within the experimentally applied photon energy range and that, (ii) as mentioned in section 2.1 ("Energy Transfer Processes in the Metal Substrate"), the high excitation densities of most experiment lead to more rapid electron thermalization times than is the case at lower fluences due to phase space arguments.[31,32,37] Unfortunately, only a few examples exist in the literature where the electron thermalization time, τ_{therm}, is measured directly by photoemission. For example, Lisowski et al.[35] obtained for ruthenium $\tau_{therm} \approx 100$ fs at fluences of ≤ 0.6 mJ/cm^2, and Fann et al.[31,32] reported for gold correponding times of about 670 and 1300 fs at even lower fluences of 0.3 and 0.12 mJ/cm^2, respectively. Extrapolation to typical fluences used in surface femtochemistry is, however, not straightforward.

Finally, it should be noted that in order to assert a genuine wavelength dependence of an ultrafast surface reaction, the different penetration depth of the exciting laser pulse has to be accounted for.[85] For instance, a shorter penetration depth of a pulse of comparable fluence causes a higher electronic temperature near the substrate surface than in the case of a deeply penetrating pulse of different wavelength. Consequently, the higher electronic surface temperature of the less penetrating pulse results in a higher reaction yield and may mask a potential resonance character of the excitation step.

5.5. Energy Partitioning into Different Degrees of Freedom

Investigations on the energy partitioning among different (translational, vibrational, rotational) degrees of freedom of the reaction product in a surface reaction offer additional insights into the underlying excitation mechanism and the pathway of energy flow. Under reaction conditions close to thermal equilibrium, for example, in temperature-programmed desorption or nanosecond-laser pulse excitation, *nonactivated* reaction systems [e.g., H_2 + Pd(100)][86,87] typically show an equally balanced energy partitioning, while the reaction proceeds adiabatically on the electronic ground state. In contrast, *activated* systems [e.g., H_2 + Cu(100) or Cu(111)][88−90] typically exhibit an energy content of the reaction product that is unequally distributed among the different degrees of freedom. Depending on the location of the reaction barrier in the entry or exit channel (referred to as "early" and "late" barrier, respectively) of the electronic ground state, translational or vibrational excitation may facilitate the reactants to overcome the transition state.[91] The topology of the PES also determines to which extent in a recombinative desorption reaction the initial excitation normal to the surface at an early stage of the reaction might be converted to lateral and ultimately to interatomic motion, that is, vibration.

Nonadiabatic effects, however, can also result in an unequal energy transfer into different degrees of freedom of the reaction product as seen, for instance, in experiments on the associative desorption of N_2 from Ru(0001) by Diekhöner et al.[10] In these studies, contrary to expectations for an early barrier, the nascent N_2 molecules carry only little vibrational energy. Apparently, they lose most of their energy on their way beyond the reaction barrier, which was explained by strong nonadiabatic coupling of the vibrational coordinate to electron−hole pairs. Up to now, only a few examples of femtosecond-laser, that is, nonequilibrium, excitation experiments in conjunction with measurements of final-state energy distributions exist. Almost exclusively, these studies have focused on the desorption of molecularly adsorbed diatomic species such as CO from Cu and NO from Pd or Pt and also NO from the metallic oxide NiO.[23,48,66,81,92] Very recently, Wagner et al.[52] published a comprehensive study on the energy partitioning also within a bimolecular association reaction, D + D → D_2 from Ru(001). This report, furthermore, represents one of the few examples of (successfully) establishing a complete energy balance among all relevant degrees of freedom in a femtochemical reaction.

The following subsections will treat the external and internal energy content of the reaction product molecule separately, while a final subsection will cover the excitations of the underlying substrate. These degrees of freedom, however, are most difficult to quantitatively account for and comprise lattice excitations such as surface reconstruction and phonon generation and also electronic excitations such as formation of electron−hole pairs.

5.5.1. Translational Energy of Desorbing Particles

To obtain information on the partitioning of excess energy in a photodesorption process that is transferred to *external*, that is, translational, degrees of freedom of the product molecule, one has to determine the velocity of the particles that leave the surface. The velocity distribution, $P_v(v)$, corresponds to a particle flux, that is, number of desorbing molecules under a certain angle to the surface normal per unit area and time. Usually the arrival time distribution of these molecules, $I(t)$, is recorded after a flight distance d by a quadrupole mass spectrometer (QMS). However, since a QMS device measures the particle density rather than the flux and faster particles spend less time in the detection volume than slower ones do,[93] this difference in detection probability needs to be accounted for by weighting the density distribution, $\rho(t)$, with the respective velocity, v. Transforming from the density to the flux domain, that is, $\rho(t)$ to $P_v(v)$, yields[20,94]

$$P_v(v) = \frac{t^2}{d} I(t) \propto \frac{1}{v} \rho(t) \tag{9}$$

Translational energy distributions are often characterized by the mean translational energy, $\langle E_{trans} \rangle$, which can be conveniently derived from the experimental QMS signal, $\rho(t)$, via the second moment, M_2, of this density distribution. M_2 is obtained by numerical integration of the measured discrete data points according to

$$M_2 = \int v^2 P_v(v)\, dv = \frac{d^2 \int t^{-3} \rho(t)\, dt}{\int t^{-1} \rho(t)\, dt} \tag{10}$$

With this moment, the $\langle E_{trans} \rangle$ can be expressed as

$$\langle E_{trans} \rangle = \int_0^\infty E_{trans} P_v(v)\, dv = \frac{1}{2} m M_2 \tag{11}$$

where m is the mass of the desorbing particle species. It should be noted here that the evaluation of the mean translational energy does not depend on a specific fit function to the experimental TOF distribution. Nevertheless, fit functions such as the empirically modified Maxwell−Boltzmann distribution

$$P_v(v)\,dv \propto v^3 \exp\left[-\frac{m(v-v_0)^2}{2k_BT}\right] dv \qquad (12)$$

are frequently used to reproduce an experimental TOF data set. For practical reasons, the initial velocity, v_0, has been introduced, since it provides more flexibility in the fitting routine. Equation 12 can be interpreted as a thermal distribution at temperature T superimposed on a stream velocity v_0 as produced, for instance, by a supersonic free jet expansion. Furthermore, a translational temperature, $T_{trans} = \langle E_{trans}\rangle/(2k_B)$ can be assigned to a TOF spectrum to characterize the translational energy content of a desorbing particle flux.[20,94,95] The factor of 2 in the denominator of this expression originates from the density-to-flux conversion (which sometimes leads to confusion).[96]

An additional general remark concerns potential collisions between particles immediately after desorption and before detection. Especially, (femtosecond) pulsed laser-induced desorption might lead to very high spatial densities of the reaction products in front of the surface due to the (ultra)-short time window in which desorption occurs [typically within a few picoseconds, e.g., 1 ps for H_2 and 10 ps for CO desorption from Ru(001)[37,38]]. Resulting collisions can then cause a change in the angular distribution[95] depending on the excitation density, that is, desorption yield. As a consequence of the changed angular distribution, the translational energy along the surface normal increases due to nozzling effects. Thus the $\langle E_{trans}\rangle$ experimentally measured generally represents only an upper bound on the initial excitation of the translational degree of freedom in a desorption reaction.[97]

For two exemplary fluences, Figure 14, top panel, displays TOF spectra of desorbing D_2 molecules resulting from single femtosecond-pulse excitation of the Ru(001) surface covered with a monolayer of atomic deuterium.[52,57] The mean translational temperatures derived from these spectra are strikingly high and exceed ~2000 K. Such temperature values of 2000 K are much higher than one would expect for thermally induced desorption, which occurs for the hydrogen recombination on Ru(001) in a temperature range of 250−450 K.[98] That the high T_{trans} of the D_2 molecules indeed indicates a reaction mechanism of this femtosecond-laser-induced process different from thermal excitation can be explained by the following comparison: For excitation conditions of $\langle F\rangle \approx 50$ J/m^2 (lower fluence data in Figure 14), 2TM calculations (see section 2.1) predict peak phonon temperatures well below 1000 K. Consequently, a phonon-induced reaction occurring at peak phonon temperatures would result in translational energies smaller by at least a factor of 2 than those observed. Higher translational energies could then only be rationalized by assuming a considerable barrier in the desorption process, which, however, disagrees with the kinetics of adsorption and thermal desorption[98] and also with the barrier height obtained by recent DFT calculations.[53]

As also clearly seen from the TOF spectra in Figure 14, the maximum D_2 desorption flux and the entire distribution itself shift to shorter flight times with increasing laser fluence, $\langle F\rangle$. This trend is illustrated in more detail in the lower panel of Figure 14. Here, the mean translational energy, $\langle E_{trans}\rangle/(2k_B)$ of H_2 and D_2 is plotted as a function of $\langle F\rangle$ exhibiting a similar fluence dependence for both isotopes.[52] This study by Wagner et al. also shows for the first time a significant

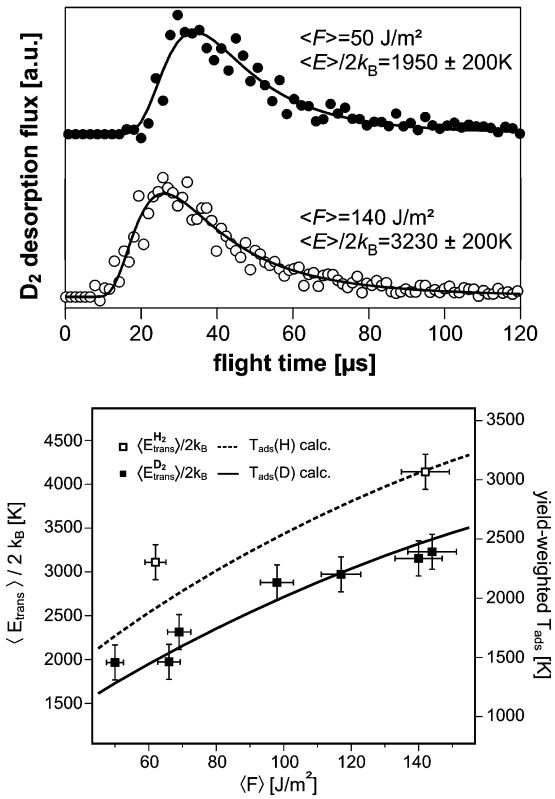

Figure 14. Time-of-flight measurements of hydrogen desorbing from Ru(001) after femtosecond-laser excitation. (top) Arrival time distributions of desorbing D_2 for two exemplary yield-weighted laser fluences, $\langle F\rangle$, together with modified Maxwell−Boltzmann fits (solid lines). Reprinted from ref 57, Copyright 2005 with permission from Elsevier. (bottom) Translational energies, $E_{trans}/(2k_B)$, obtained from time-of-flight spectra for D_2 and H_2 as a function of $\langle F\rangle$. Solid and dashed lines indicate the yield-weighted adsorbate temperature, T_{ads}^{YW}, of a H and D layer, respectively, where $T_{ads}^{YW} = \int_0^\infty T_{ads}(t)R(t)\,dt/(\int_0^\infty R(t)\,dt)$. Note that both experiment and model show a clear isotope effect and agree in the trend of increasing translational energy with increasing fluence. However, the right axis (T_{ads}^{YW}) has to be scaled with a factor of 1.35 to match the experimental data for $\langle E_{ads}/(2k_B)\rangle$. Reproduced with permission from *Phys. Rev. B* (http://link.aps.org/abstract/PRB/v72/e205404), ref 52. Copyright 2005 American Physical Society.

isotope effect in the excitation of the translational degree of freedom during a femtosecond-laser-induced surface reaction. Furthermore, such a translational energy-vs-fluence plot (Figure 14, lower panel) can be used to estimate the minimum energy released into translation. Extrapolation of $\langle E_{trans}\rangle/(2k_B)$ to zero fluence yields the axis intercept for the translational energy solely due to the effective ground-state barrier, which in the case of the hydrogen recombination from Ru(001) is in reasonable agreement with theoretical calculations.[52,53,99,100] As far as model calculations of the energy transfer during an ultrafast laser-induced surface process are concerned, it is interesting to note that an empirically introduced adsorbate temperature, T_{ads}^{YW} (the temperature T_{ads} obtained from 2TM and friction calculations and then weighted with the respective desorption yield), qualitatively reproduces the translational temperatures measured in the experiments.[52] Details on the success and limitations of these one-dimensional friction calculations usually applied to describe a femtosecond-laser-induced surface process will be discussed in section 6.1. "Multidimensional Dynamics".

5.5.2. Vibrational and Rotational Energy Distribution

Measurements of the energy content in *internal* degrees of freedom of the desorbing product species, like vibration and rotation, require state-selective investigations [for example, REMPI (resonance-enhanced multiphoton ionization) or LIF (laser-induced fluorescence)][101] of the photodesorption process. Usually the REMPI technique is applied, whereby the surface reaction is initiated by an ultrashort pump pulse followed by nanosecond detection pulses of one or more colors, which then ionize the product molecules after a short flight distance (in the millimeter to centimeter range) in front of the surface (see experimental setup in the lower panel of Figure 7). Scanning the resonant excitation wavelength with a fixed ionization wavelength maps the initial rovibrational population distribution onto the ion signal of the desorbing particles. The rotation (J)- and vibration (v)-dependent state population, $N(v,J)$, can then be determined if the overall transition probabilities comprising the electronic transition moments, the vibrational wave function overlap (Franck−Condon factors), and the angular momentum- and the polarization-dependent correction factors are known (e.g., see ref 52). In addition, all REMPI schemes exploiting one-photon transitions in the resonant excitation step, that is, all $(1 + x)$ excitation schemes, allow for obtaining information on the molecular alignment of the desorbing particles. Here, the molecular polarization, $P = (I_{||} - I_{\perp})/(I_{||} + I_{\perp})$, is measured, where $I_{||}$ and $I_{\perp}$ denote the ion intensity obtained for parallel and perpendicular, respectively, laser polarization of the resonant excitation step with respect to the surface normal.[54] The rotational alignment factor, $-1 \leq A_0^{(2)} \leq 2$, inferred from P depending on the rotational branch[102] then describes the preferential motion while the desorbing molecule leaves the surface; a positive $A_0^{(2)}$ implies a preference for a helicopter-like rotation, whereas $A_0^{(2)} < 0$ indicates a more cartwheel-like motion.[52,54,102]

The conclusions on the energy partitioning during a desorption reaction, which one can draw from the analysis of the normalized populations, $N(v,J)$, as a function of either the rotational or the total internal energy, are the following: In a semilogarithmic representation, these so-called "Boltzmann plots" should exhibit a linear slope for a molecular ensemble in thermal equilibrium. This slope is inversely proportional to the rotational temperature, T_{rot}. Deviations from the linear behavior may underline the strong nonequilibrium conditions prevailing in a femtosecond-laser-induced reaction. However, one should note that to some extent those deviations can also originate from dynamical effects present even in thermal reactions.[54,103] Overpopulation of low rotational states, that is, rotational cooling, can be rationalized by steering forces acting during an adsorption process. Low-J molecules are more readily steered into a favorable orientation through the PES landscape than species in high J states. Consequently, due to the principle of detailed balance, this results in a higher desorption probability for molecules with low rotational excitation. In addition, vibrational heating might be observed, an effect in nonactivated or only slightly activated systems, which can be explained by the adiabatic lowering of the vibrational frequencies upon dissociation. In the time-reversal, the association reaction, the nascent molecule is excited to higher vibrational levels.[104]

In hot-electron driven reactions, where desorption of a *molecular* adsorbate like NO or CO is initiated by femtosecond-laser pulses, a pronounced vibrationally nonthermal excitation of the product is found.[23,48] For the NO desorption from Pd(111) reported by Prybyla et al.,[23] the high energy content in the internal N−O stretch vibration was attributed to transient (multiple) population of the antibonding NO π^* orbital, which marks the different desorption mechanism compared with thermal equilibrium. However, as Cai et al.[78] pointed out, a similar argument for the femtosecond-laser-induced CO desorption from various metal surfaces based on the population of the $2\pi^*$ state fails since these states lie too high to be effectively occupied by 800-nm laser excitation. However, other short-lived antibonding states at lower energy resolve this seeming contradiction and provide the means for efficient electronic excitation of the CO adsorbate.[78] To summarize both molecular systems mentioned so far [NO/Pd(111)[23] and CO/Cu(100)[48]], the obtained highly elevated vibrational temperatures reflect the high temperature of the *electronic* system. It should be noted that these T_{vib}'s of $\geq$2000 K could only be observed because the intramolecular stretch vibration of these molecules remains rather undamped in the desorption exit channel; that is, the respective population of the nascent molecules is preserved all the way into the gas phase.

In contrast, the associative desorption of D_2, that is, the recombination of two hydrogen *atoms* from Ru(001), by Wagner et al.[52] exhibits a rather low excitation of the vibrational degrees of freedom and even less in the rotations. The translational degree of freedom was found to be predominantly excited with an energy ratio among translation, vibration, and rotation scaling as 5.4:1.3:1. An explanation for the observed much higher translational energy compared with vibration could be given very recently by DFT multidimensional friction calculations by Luntz et al.[53] The ground-state topology causes this difference in energy partition rather than a preferential frictional coupling into one or the other coordinate. Details will be given in section 6.1. In addition, Wagner et al.'s work on D_2/Ru(001) represents the only measurement of the molecular alignment of a femtosecond-laser-induced desorption reaction. The authors found a substantial but laser-fluence- and quantum-state-independent positive alignment ($A_0^{(2)} = 0.27$), which means that a predominantly helicopter-like motion is involved while the D_2 leaves the Ru surface.

A final remark again concerns possible collisions that might falsify the reported results on the energy partitioning during an ultrafast surface reaction as mentioned before. However, the various experimental results obtained, especially for the D_2/Ru(001) system, such as the incomplete rotational thermalization, a nonzero molecular alignment, and no evidence of a nozzling effect in the TOF spectra, that is, narrowing of the velocity distribution with increasing laser fluence, indicate that collisional distortions after desorption do not occur to a significant extent in the reported experiments.[52]

5.5.3. Substrate Degrees of Freedom

Besides the desorbing product particle, which carries away energy in external and internal degrees of freedom, also the remaining substrate may take up a non-negligible partition of the entire energy available during a desorption process. For a quantitative analysis, it is helpful to establish an energy balance comprising the various degrees of freedom. One successful example of such energy balancing in a femtosecond-laser-induced desorption reaction is again given by Wagner et al.[52] for the D/Ru(001) system. The overall mean

energy of the desorbing D_2 particle flux given by $\langle E_{flux}\rangle = \langle E_{trans}\rangle + \langle E_{vib}\rangle + \langle E_{rot}\rangle = 2k_BT_{trans} + k_BT_{vib} + k_BT_{rot}$ was found to almost perfectly agree with the energy corresponding to the calculated yield-weighted adsorbate temperature, T_{ads}^{YW}, as introduced in section 5.5.1. Given that in the electronic friction model one assumes a time-independent and one-dimensional friction coefficient, η_{el}, together with a single adsorbate temperature, T_{ads}, which uniformly characterizes the adlayer, these matching temperatures appear rather astonishing, which will be discussed in more detail in section 6.1 ("Multidimensional Dynamics"). At least, this matching energy balance seems to indicate that in the H/Ru femtochemistry no substantial energy partition is omitted.

In contrast, adsorption and desorption experiments on hydrogen/silicon (although being a non-metal system) demonstrate the importance of substrate degrees of freedom in a prototypical manner. Extremely small sticking probabilities at room temperature together with a strong dependence of the sticking coefficient on the surface temperature[105] on one hand and remarkably small translational energies of the desorbing D_2 molecules[106] on the other hand were initially considered as arguments to question the applicability of the detailed balance principle for the H(D)/Si system.[106] To reconcile these observations, strong distortions of the silicon lattice in the transition state were proposed and also theoretically predicted.[107] In adsorption experiments, molecules impinging on a relatively cold surface encounter the substrate atoms in a configuration that is unfavorable for dissociation and, hence, experience a high adsorption barrier (resulting in small sticking probabilities). At elevated surface temperature, the incident molecules have a chance to encounter rearranged substrate atoms in a more favorable configuration and dissociate more easily (so-called "phonon-assisted sticking").[107] In the reverse process of recombinative desorption, most of the excess barrier energy is released into phonon excitations of the substrate. In addition, molecular beam studies with SHG detection of the hydrogen coverage by Dürr et al.[108] showed that both the Si surface temperature and translational energy of the adsorbing H_2 molecules influence the sticking probability. Consequently, it was suggested that the activation in the lattice *and* molecular degrees of freedom are dynamically interconnected. It is now commonly accepted for the H/Si system also through many other experiments, for example, refs 109 and 110, that the principle of detailed balance is very well applicable if excitations of substrate phonons are included in the energy partitioning.

One further example that substrate lattice excitations during desorption crucially influence the entire reaction is found in femtochemistry studies on Cs/Cu(111) by Petek et al.[22,111,112] Ultrafast laser-induced charge transfer of an electron from the metal substrate into an unoccupied resonance of the alkali atom induces nuclear motion of both the adsorbate *and* the substrate atoms via the repulsive Coulomb force. The evolving wave packet dynamics have been monitored by these authors in great detail through the accompanying changes in the surface electronic structure by 2PPE. In this adsorbate−substrate motion, the high mass of Cs (133 amu) leads to dynamic recoil[113] of the underlying Cu atoms (63 amu), and hence the Cs atom cannot gain enough kinetic energy in the ultrashort excited-state lifetime (∼20−50 fs) to escape from the deep adsorption well.[112] Even changing the atomic mass ratio of the adsorbate vs the substrate to more favorable values to reduce the recoil and hence the substrate excitation has not led to a successful detection of desorption products, for example, for the Na/Cu and K/Pt systems by Watanabe and Matsumoto.[114] However, with a highly improved detection sensitivity (based on an integrating thermal ionization detector), Petek et al.[112] have reported in a short note a proof of principle for Cs desorption in such experiments, yet with a yield still too small for quantitative measurements.

Finally, electronic excitations such as electron−hole pairs represent important substrate degrees of freedom. As briefly mentioned before, one of the most prominent examples here is Diekhöner et al.'s work[10] on the associative desorption of N_2 from Ru(001). In internal state and translational energy resolved experiments, the authors measured only little vibrational excitation in the nascent N_2 molecule. This is especially surprising, since the N/Ru(001) ground-state PES shows a high vibrational barrier of 2−3 eV.[115,116] Furthermore, the desorbing N_2 carries only $\sim^1/_3$ of the barrier energy; that is, roughly $^2/_3$ of the desorption energy is lost to the surface in desorption. These findings imply strong vibrational quenching (cooling) in reactive trajectories passing the barrier and consequently were taken as (indirect) evidence for strong nonadiabatic coupling in the N_2 desorption process.

5.6. Adsorbate Interactions with Chemical Surroundings and Local Structure

Reactants adsorbed on a solid surface interact with their surroundings, both with other neighboring reactants, which eventually leads to the chemical reaction, and with those adsorbates that do not directly participate in the chemical reaction but modify the electronic structure. In addition, as *the* foundation of heterogeneous catalysis and as the topic of this paper, the interaction of the reactants with the underlying (metal) substrate is essential and might significantly depend on the local structure, for example, the adsorption site. In the following, exemplary consequences arising from various aspects of these interactions will be briefly discussed: (i) adsorbate−adsorbate interactions, (ii) the influence of adsorbate coverage, and (iii) site-specific interactions.

(i) Adsorbate−adsorbate interactions play a crucial role in the femtosecond-laser-induced hydrogen recombination on Ru(001). Denzler et al.[38] report experiments with isotopically mixed hydrogen adlayers consisting of both H and D. Starting with a saturation coverage but with varying proportions of both isotopes, the total yield of all three product molecules, H_2, D_2, and HD, was measured for both the thermally induced recombination and the reaction induced by ultrafast laser excitation. While under thermal equilibrium conditions, the desorption yields of all three isotopomeres follow second-order reaction kinetics, the corresponding yields induced by femtosecond-laser excitation demonstrate that the "mere" presence of one isotope enhances or hinders the reaction of the other isotope. For instance, the D_2 recombination yield is substantially enhanced if H is coadsorbed. This so-called "dynamical promotion" effect is attributed to the faster energy transfer from the Ru substrate to a H adsorbate than to the heavier D due to the electronic nature of the coupling process. Note that the electronic coupling time as the inverse of the friction coefficient scales proportionally with the reactant's mass; hence $\tau_{el}(H_2) = {}^1/_2\tau_{el}(D_2)$, see section 2.2. Consequently, a surrounding of a D atom consisting of H atoms is more rapidly vibrationally

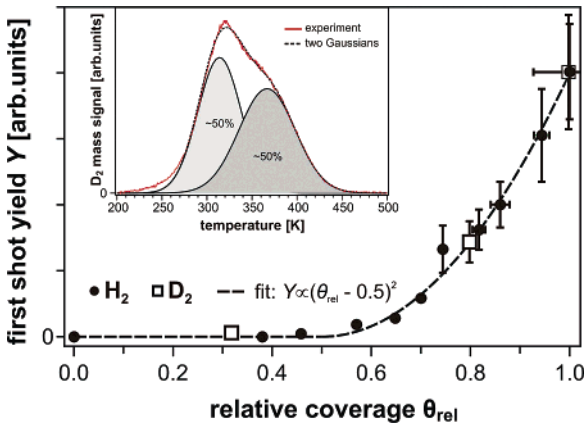

Figure 15. Coverage dependence of the femtosecond-laser-induced hydrogen recombination from Ru(0001) at an absorbed fluence $\langle F \rangle$ of 60 J/m^2. Apparently, both H_2 and D_2 obey the same Y vs θ_{rel} relationship. Adsorbate interactions are believed to cause a nearly threshold-like behavior with yields detectable only above $\theta_{rel} = 0.5$. The quadratic dependence of the yield on coverage for $\theta_{rel} \geq 0.5$ is empirical (dashed line). The thermal desorption spectrum for D_2/Ru(0001) shown in the inset exhibits two components with a second maximum above $\theta_{rel} \approx 0.5$. This corroborates significant adsorbate interactions leading to differences in the activation energies for desorption. Adapted with permission from ref 18. Copyright 2004 American Chemical Society.

excited and starts earlier exploring locations on the surface that favor the recombination of neighboring D reactants compared with a matrix of surrounding D atoms, which remains still relatively cold due to slower excitation. A physical picture of this effect would involve attractive and repulsive interactions between the faster excited H atoms and the two D reactants. Also electronic changes in the adsorbate−substrate complex might contribute. The transient influence of the reactants' surrounding may alter the activation energy, shift the excited PES involved in the desorption process, or both. Hence the rate constant is changed, which in a more general way for a bimolecular surface reaction (such as an associative desorption) can be reformulated as

$$A_{ad} + B_{ad} \xrightarrow{k[U(t)]} AB$$

with $U(t)$ describing the time-dependent surroundings.[38,57] In moments of preferential adsorbate−substrate conditions, a favorable energy landscape is created, which leads to reaction. This microscopic picture also complies with thermally initiated surface reactions, in which statistical fluctuations cause the respective surrounding conditions.

(ii) Denzler et al. showed in a further publication[18] that these adsorbate−adsorbate interactions in the femtochemistry of hydrogen/Ru(001) also manifest themselves in a peculiar coverage dependence of the desorption yield from isotopically pure H or D layers as shown in Figure 15. Only for coverages θ above a threshold of ~0.5 ML, the desorption yield rises above the detection limit and reaches its maximum at the saturation coverage of $\theta = 1$ ML. Possible origins are the coverage dependence of the binding energy or of the electronic friction coefficient, but also the influence of the significantly lower barrier for diffusion at low coverage has been discussed recently.[117] The latter might prevent successful recombination events even at coverages with nearest neighbors such as at $\theta = 0.5$ ML. Why, however, this threshold of femtosecond-laser-induced recombination occurs at that particular coverage of $\theta = 0.5$ ML cannot be explained by diffusion but is consistent with the following observation in thermally induced recombination.

In thermal desorption, interesting evidence is found for distinct adsorbate−adsorbate interactions in the hydrogen/ruthenium system. The TD spectrum of 1 ML D_2 from Ru(001) (see inset of Figure 15) exhibits a twofold feature, a characteristic maximum at 320 K and a shoulder around 380 K.[38,98] Unlike the initial interpretation of the TDS data according to which the two desorption peaks originate from adsorbates on two different adsorption sites,[98] it is now commonly accepted that hydrogen atoms on Ru occupy the 3-fold coordinated sites at *all* coverages[118] and that the shape of a hydrogen TD spectrum is caused by increasing adsorbate−adsorbate interaction at higher coverages. As also demonstrated in the inset of Figure 15, two Gaussians of approximately equal integrated area give a good fit to the TDS data. Apparently, for both the thermally and the femtosecond-laser-initiated recombination reaction, lateral interactions within the adsorbate layer become important for coverages $\theta > 0.5$ ML.

Generally, coverage-dependent surface chemistry can originate from direct attractive or repulsive adsorbate−adsorbate interactions or coverage-dependent changes in the electronic structure of the adsorbate−substrate complex. Related effects are known in promotion and poisoning effects in heterogeneous catalysis due to coadsorption of other adsorbate species that change the electronic structure.[119] For small adsorbates such as hydrogen, however, steric repulsion between neighboring sites can be neglected and indirect, that is, substrate-mediated, interactions dominate.[120,121] For example, H-coverage-dependent photoemission experiments from Ni and Pd reveal pronounced changes in the band structure of the metal substrate even at low coverages.[122] Such changes in the electronic structure may also affect the electronic friction coefficient and hence the coupling time, τ_{el}, for energy flow into the adsorbate coordinate. Therefore, both a coverage-dependent friction coefficient and changes in the adsorbate binding energy may contribute to the reported coverage dependence of the femtosecond-laser-induced hydrogen desorption yield from Ru. Additional corroboration for the importance of adsorbate−adsorbate interactions is found in scanning tunneling microscopy (STM) studies by Mitsui et al.[123] on the dissociative adsorption of hydrogen on Pd(111), the time reversal of associative desorption. The authors found that for a successful adsorption event not only both reactants (i.e., the two H atoms) but also the surroundings play a crucial role. The adsorbing H_2 molecule seems to require, contrary to conventional thinking, more than the necessary two-vacancy sites on the Pd surface for an effective reaction.

Summarizing that part of adsorbate interactions that cause a clear coverage dependence of the photoreaction, it is noteworthy that care should be taken in experiments where diffusion of the reactants within or between subsequent excitation pulses might occur. For example, Fournier et al.[124,125] reported a dramatic 5 orders of magnitude probability increase in the femtosecond-laser-induced CO desorption from Pt(111) when the coverage is increased only by a factor of 5. While these authors initially tried to rationalize this phenomenon in terms of increasing lifetimes of the electronic excitation, Roeterdink et al.[126] pointed out that diffusion and hence refilling of the laser-depleted spot on the sample is non-negligible. In addition, effects due to the strong dipole−dipole coupling of the CO had not been taken into account,

which might have contributed to this dramatic variation in desorption probability.[127] Only all-optical pump−probe experiments with a sufficiently larger pump beam diameter with respect to the probe beam and single-shot optical excitation with subsequent mass spectrometry measurements are not biased by diffusion.[125]

(iii) The site-specific nonlinear optical response of the adsorbate−substrate system offers the possibility to trace a surface process such as diffusion between different classes of adsorption sites, for example, step and terrace sites. Typically, nonlinear optical spectroscopy methods are applied, which monitor changes in either the electronic structure of the substrate or the intramolecular adsorbate vibrations due to different interaction strength with the substrate upon diffusion. While the former was exploited in the already cited femtosecond-laser-induced O/Pt(111) diffusion experiments of Stépán et al.,[51,74] the latter provides the base for the time-resolved pump−probe vibrational spectroscopy of the CO diffusion on Pt(533) by Backus et al.[59] A more detailed description of both will be given further below; Stépán et al.'s work is covered in section 6.1, "Multidimensional Dynamics" and Backus et al.'s study in the next section 5.7, "Real-Time Studies".

5.7. Real-Time Studies

Following a chemical reaction in real time by ultrafast spectroscopy has always been a major goal and challenge in surface reaction dynamics. In surface femtochemistry, two experimental approaches to study the dynamics in real time have been employed. (i) In two-pulse correlation experiments (see section 5.2.), the system response, for example, the reaction yield, after the excitation with a pair of pulses is traced as a function of their temporal separation. These studies provide information on the time scales of energy flow between different degrees of freedom, for example, the coupling time of the adsorbate motion to the substrate electronic transient. (ii) In all-optical pump−probe experiments, the reaction is triggered by an ultrashort pump pulse, and the reactants' response is monitored by a molecule-specific probe such as vibrationally resonant SFG. However, accumulation of reaction products and interfering signal contributions from both the substrate and the adsorbate make this kind of experiments rather difficult to perform. Both types of experimental approaches clearly work in the time domain but provide complementary information on an ultrafast time scale. While the two-pulse correlation ("pump−pump") measurements permit access to the energy flow in the system, the pump−probe studies monitor the time evolution of the system along the reaction coordinate initiated by a single pump pulse. We will first discuss the latter type of experiments.

In 1992, first attempts were done by Prybyla et al.[128] for the ultrafast-laser-induced CO desorption from Cu(111). The authors measured the second harmonic (SH) response after a strong pump pulse has excited the Cu surface. After less than 350 fs, the SH signal again had reached the baseline level, wherefrom it was concluded that the desorption event is complete by that time. However, since such a nonlinear optical SH response depends on both the change of electronic structure due to desorption of the molecule and the transient electronic excitation of the substrate, the contribution solely due to the chemical reaction is rather involved and thus a molecule specific probe of the reactants would be beneficial.

In this way, another $\chi^{(2)}$ (second order nonlinear susceptibility) spectroscopy based on sum-frequency generation (SFG) offers molecular specificity by resonant enhancement of adsorbate vibrations. As in SHG, also SFG is surface-sensitive since only for broken centrosymmetry $\chi^{(2)}$ is nonvanishing (in dipole approximation). Important contributions to applying time-resolved SFG to surface processes were achieved, for instance, by Bandara et al.[129,130] and Kubota et al.[131−133] in a variety of different systems, however, exclusively with a time resolution of several (tens of) picoseconds. Among these are investigations on the decomposition dynamics of formate (CHOO) on NiO(111),[129] transient melting and recrystallization of D_2O on CO/Pt(111),[131] diffusion of CO within CO/Ni(111),[132] and phase transitions of cyclohexane (C_6H_{12}) layers adsorbed on Ni(111).[133] Although the time resolution was sufficient for some aspects of these surface processes, for example, the detection of unstable intermediates in the formate decomposition,[129] these experiments mainly monitor thermal equilibrium conditions, which undergo a laser-induced T (temperature) jump. These studies will not be discussed in more detail here because this review is dedicated to femtochemistry.

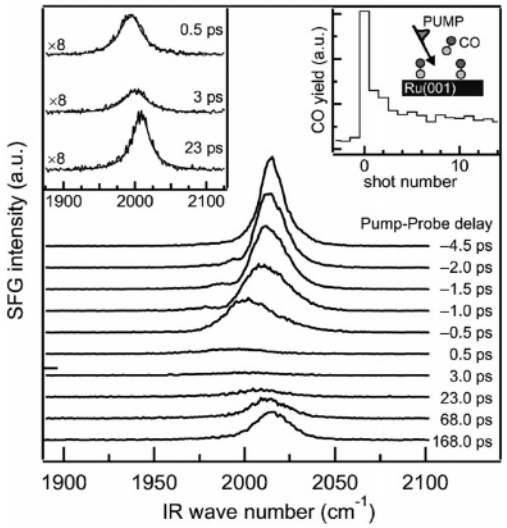

Figure 16. Time-resolved SFG spectra of the C−O stretch vibration under desorption conditions (absorbed laser fluence 55 J/m^2) as a function of the pump−probe delay. The transient red-shift and the decrease in intensity are magnified in the left inset. The right inset demonstrates the high desorption probability of ~50% for the first shot. Reprinted with permission from *Phys. Rev. Lett.* (http://link.aps.org/abstract/PRL/v84/p4653), ref 60. Copyright 2000 American Physical Society.

Pioneering work on time-resolved studies of surface reactions by means of femtosecond vibrational SFG spectroscopy was conducted by Bonn et al.[60] Using the so-called IR broadband vibrational SFG spectroscopy,[60,134] where the IR pulse with femtosecond duration covers a vibrational region of ~150 cm^{-1}, allows simultaneously detection of a respectively wide vibrational spectrum, in principle in a single shot. Applying this technique as a probe of femtosecond-laser-excited CO/Ru(001), Bonn et al.[60] observed a substantial transient red-shift, a broadening of the C−O stretch resonance and a strong decrease in intensity at a fluence that causes efficient desorption of the CO molecules (see Figure 16). These findings could be explained in terms of anharmonic coupling of the intramolecular stretch vibration to external low-frequency modes such as the frustrated translation and also especially the frustrated rotation. Since the detected SFG signal originates from CO species still remaining on the surface, the conclusions on the desorption

dynamics are rather indirect. Roke et al.[135] showed in a later publication that it remains difficult to quantitatively identify the fraction of CO molecules that indeed leave the surface during the photostimulated reaction. Similar time-resolved SFG studies with subpicosecond time resolution were undertaken also by Fournier et al.[71] for the CO desorption from Pt(111) and by Symonds et al.[70] for CO/Ru(10$\bar{1}$) (see Table 1).

As already pointed out, in such desorption experiments, the actual reactants undergoing the chemical/physical (adsorption-to-gas phase) transformation cannot be traced along the entire route from the initial (equilibrium) state to the product state. However, diffusion experiments for adsorbates with distinctly different adsorption sites allow such monitoring. Recently, two different groups carried out studies on the ultrafast-laser-induced lateral motion of an adsorbate on stepped Pt surfaces [O on Pt(111)[51,74] and CO on Pt(533),[59] respectively]. In both cases, the stronger interaction of the adsorbate with the Pt substrate at step sites leads to an initial occupation of the steps at low coverages under equilibrium conditions, while the femtosecond-laser excitation then causes the O and CO, respectively, to diffuse onto the terraces. Although Stépán et al.[51,74] used the species unspecific SH spectroscopy to monitor the photoinduced diffusion, the authors still could extract the hopping probability of the oxygen adsorbate since the SH signal unambiguously depends on the step coverage. Note that these time-resolved SHG studies represent a demonstration of two-pulse correlation measurements, which probe the energy flow in a diffusion process.

Complementarily, Backus et al.[59] applied the adsorbate vibration-sensitive SFG method in a time-resolved pump−SFG−probe configuration to follow the photoinduced CO diffusion. Again, due to the different interaction strength of the CO adsorbate with the Pt surface for step vs terrace sites (reflected in different binding energies), the intramolecular C−O stretch resonance is blue-shifted as the CO hops from the steps to the terraces (see Figure 17, panel a). As shown in panel b of the same figure, the SFG intensity arising from step species is depleted as a function of pump−probe delay. A corresponding increase in the terrace signal, however, is not as clearly noticeable due to contributions from dipole−dipole coupling to the SFG signal.[136] The main insights Backus et al.[59] could gain from their real-time observation of the CO diffusion concern the questions of which specific vibrational modes are involved in the overall reaction and on what time scales these processes occur. For surface diffusion, intuitively one would expect that the adsorbate needs sufficient excitation in a direction parallel to the surface for hopping to occur from one adsorption site to the next. Thus it seems that only the frustrated translational mode is responsible for CO diffusion. But Backus et al. showed that the situation is more complex. Calculations of the hopping probability derived from transient temperatures for the substrate electrons and the CO frustrated translational and rotational modes show that, contrary to usual expectations, the excitation of the frustrated *rotation* is essential in the CO diffusion process (see Figure 17, panels c, d, and e). Energy exchange solely via excitation of the frustrated *translational* mode is significantly too slow to cause the hopping motion of the CO within the ultrashort, that is, subpicosecond, time scale observed in the experiment. Thus, the work by Backus et al. shows that a simple one-dimensional view of diffusion is insufficient and that, in general, diffusing molecules perform a concerted motion like dancing a molecular waltz along the surface.[137] A similar behavior was found, for instance, in the rapid diffusion of water dimers on Pd(111) exhibiting complex multidimensional dynamics.[138]

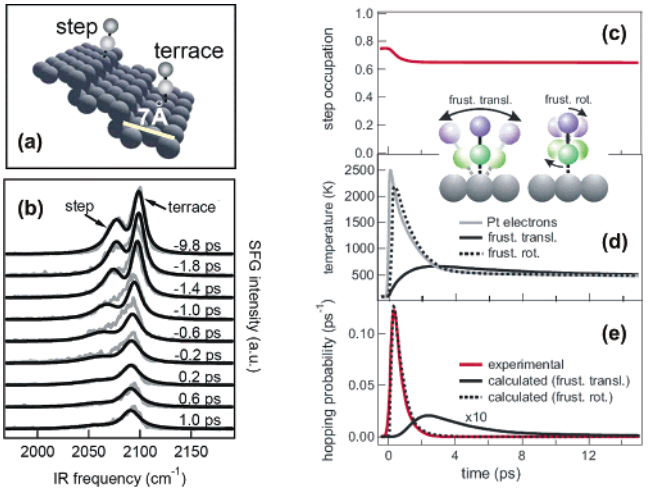

Figure 17. Real-time observation by SFG vibrational spectroscopy of the diffusive motion of molecular CO from step to terrace sites on a Pt(533) surface induced by femtosecond-laser excitation. (a) Schematic picture of the CO adsorbate on the Pt surface with four atom wide (111) terraces and monatomic (100) steps. (b) Experimental (gray) and calculated (black) transient SFG spectra for various pump−probe delays. (c) Time profile of the step site occupation after excitation with the pump pulse. (d) Electron temperature as a function of time after excitation together with the temperatures of the frustrated translational and frustrated rotational modes. Respective electronic coupling times are $\tau_{trans} = 4$ ps and $\tau_{rot} = 0.1$ ps. (e) Time profile of the experimental and calculated hopping probability. The experimental curve is obtained by differentiating the step occupation of panel c. Calculations are performed for hopping due to excitation of the frustrated translation and rotation mode using the respective time-dependent adsorbate temperatures of panel d. The inset shows the molecular motions associated with the two modes. Note that only the calculation based on the excitation of the frustrated *rotation* reproduces the experimentally derived hopping probability. Reprinted with permission from *Science* (http://www.aaas.org), ref 59. Copyright 2005 American Association for the Advancement of Science.

6. Recent Developments and Future Prospects

This section provides an overview of the current progress in the field of femtochemistry at metal surfaces, which is still an active research area after its beginning more than a decade ago. Especially, the breakdown of the Born−Oppenheimer approximation and nonadiabatic coupling as one of the dominant phenomena in surface femtochemistry is highly connected to other challenging fields such as mode-selective chemistry induced by inelastic tunneling or electron−vibrational coupling in surface reactions. The first subsection is devoted to progress made in the theoretical modeling of the elementary energy transfer mechanisms in femtochemical surface processes. It has long been a question why the frequently used one-dimensional frictional description of substrate−adsorbate coupling (see section 2.2.) is so successful especially for intrinsically multidimensional processes such as associative desorption reactions. The second subsection sets surface femtochemistry in the context of related fields, while the last subsection will cover the realm of reaction control, which is still a challenging goal to occur on surfaces.

6.1. Multidimensional Dynamics

The quantitative description of nonadiabatic coupling between the substrate and the adsorbate via (electronic) friction (as outlined in section 2.2) was originally developed to describe femtosecond-laser-induced desorption of diatomic species along the center-of-mass coordinate, which can be reduced to a one-dimensional (1D) problem.[39,40] Thus, it was not clear at all, why such a 1D model should be appropriate for an associative desorption reaction, since this process has to be viewed at least as a two-dimensional (2D) problem comprising the interatomic distance, that is, the bond length, d, and the center-of-mass distance of the diatomic product molecule from the surface, z. Nonetheless, the 1D model has been applied with (almost surprisingly) great success to the CO + O oxidation[17] and the H + H recombination on Ru(001),[18,38,52,57] both referred to several times in the previous sections. Already in the mid-1990s, Head-Gordon and Tully[61,62] developed a concept to treat multidimensional molecular dynamics with electronic frictions. Application to femtosecond-laser-induced desorption of CO from Cu(100) demonstrated the importance of frustrated rotational modes in the desorption process.

Recently, Luntz and Persson[63] extended the traditionally 1D friction model to the above-mentioned dimensions d and z of the nascent product molecules in the association reactions H + H → H_2/Cu(111) and N + N → N_2/Ru(001). A first-principle expression for the frictional tensor, η_{ij}, was obtained based on previous work on vibrational damping of adsorbates[139] and atomic adsorption[62,140] using time-dependent DFT. Furthermore, Luntz et al.[53] applied the same methodology to the comprehensively studied H/Ru(001) system. A three-dimensional (3D) model was introduced with two coordinates d and z representing the nascent hydrogen molecule, whereas the third dimension with a single phonon coordinate q described the coupling to the Ru lattice by dynamic recoil. Both the potential energy surface and the electronic friction tensor were calculated by DFT so that there are no adjustable parameters in the comparison of this model with the wide range of experimental data available for the H/Ru(001) system. In this sense, the work by Luntz et al.[53] provides a "first principles" model. Based on the molecular dynamics with electronic friction by Head-Gordon and Tully,[61,62] the 3D classical equation of motion on the PES $V(z,d,q)$ are given by the following set of coupled differential equations

$$\mu\ddot{d} = -\frac{\partial V}{\partial d} - \eta_{dd}\dot{d} - \eta_{dz}\dot{z} + F_d(t)$$

$$m\ddot{z} = -\frac{\partial V}{\partial z} - \eta_{zz}\dot{z} - \eta_{dz}\dot{d} + F_z(t)$$

$$M_s\ddot{q} = -\frac{\partial V}{\partial d} - \eta_q\dot{q} + F_q(t) \qquad (13)$$

where μ, m, and M_s are the reduced mass of the vibration, the molecular mass, and the surface mass of a Ru atom (forced oscillator), respectively. The molecular modes z and d are coupled to a thermalized electron distribution at temperature T_{el} via the frictional tensor η_{ij}, which causes damping and induces fluctuating forces $F_i(t)$ ($i = z,d$) according to the second fluctuation−dissipation theorem[141]

$$\langle F_i(t)F_i(t')\rangle = 2k_B T_{el}\eta_{ii}\delta(t - t') \qquad (14)$$

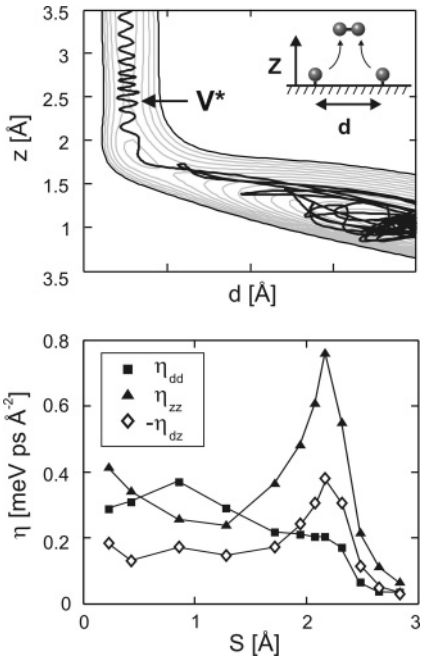

Figure 18. Multidimensional ab initio DFT and trajectory calculations for the femtosecond-laser-induced associative desorption of H_2 from Ru(001). (top) Contour plot of the 2D potential energy surface, $V(z,d)$, with 0.1 eV energy intervals. The barrier in the desorption exit channel is marked by V^*. A typical associative H_2 desorption trajectory following femtosecond-laser excitation of 140 J/m^2 adsorbed fluence is overlaid. The inset illustrates the associative desorption process. (bottom) Multidimensional friction coefficients η along the minimum energy pathway S, where $S = 0$ Å corresponds to the adsorbed state, [1 × 1]H/Ru(001), before excitation and $S = 3$ Å corresponds to the H_2 + H/Ru(001) asymptote. Note the significant differences in η near the transition state V^* at $S \approx 2$ Å. However, at times when the nascent H_2 is close to V^*, the electronic temperature has already significantly decreased. Reprinted with permission from ref 53. Copyright 2006 American Institute of Physics.

In this way, eq 14 and an analogue version for the phonon coordinate q relate the transient electronic and phononic temperatures, $T_{el}(t)$ and $T_{ph}(t)$, obtained from the 2TM to the forces driving the molecular dynamics of the photodesorption process.

Figure 18, top panel, shows a contour plot of the 2D PES $V(z,d,q = 0)$ obtained by DFT using 2 × 2 (and partially 4 × 4) Ru unit cells for the desorption of the single H_2 molecule. In the bottom panel of Figure 18, elements of the frictional tensor η_{ij} are plotted along the minimum energy path S towards desorption. As obvious from this graph, the frictional coefficients for the different coordinates are rather similar at $S = 0$, which corresponds to the initially adsorbed state where both hydrogen atoms reside on the Ru surface in equilibrium before the laser excitation occurs. On the contrary, near the transition state V^* at $S \approx 2$ Å, $3\eta_{dd} \approx \eta_{zz}$. Depending on the excitation density, that is, laser fluence, and hence the desorption probability, classical trajectories (typically between 6000 and 40 000) were run for this system in molecular dynamics calculations. Also in the top panel of Figure 18, a successful but exemplary trajectory of an H−H forming H_2 is overlaid onto the 2D contour plot of the PES. By evaluation of an appropriate number of trajectories successfully leading to desorption, most of the experimental results could be reproduced with remarkably good agreement: the two-pulse correlation, the nonlinear

fluence dependence of the desorption yield, and the isotope effect.[53]

It is instructive to inspect individual trajectories (like that of Figure 18). Most of the electron-mediated excitation of nuclear coordinates occurs at early times after the laser pulse when the system is still deep in the H−H adsorption well and much below the barrier. In this region, although $\eta_{dd} \approx \eta_{zz}$, most of the nuclear excitation occurs through the vibrational coordinate because of the four times smaller reduced mass along the coordinate d versus that along z (see ref 49 on the different notation regarding the mass-independent vs -dependent friction coefficients found in the literature). By the time the H−H approaches the barrier (where $\eta_{zz} \gg \eta_{dd}$), T_e has already cooled so that the frictional force, F_i, is small. However, even though initially most of the excitation occurs through the vibrational coordinate d, the rapid energy exchange ("thermalization") between the d and the z coordinate along the trajectory on the way to desorption conserves little memory of the mode of excitation. In this manner, Luntz et al.[53] could show that the unbalanced energy partitioning between translational and vibrational degrees of freedom observed in the experiment predominantly originates from the topology of the ground-state PES, in particular from the small but distinct barrier in the translational channel.

Besides the latter example of multidimensional dynamics, where the rapid energy exchange between modes allows a reduction to a single reaction coordinate, a further example of a limiting case of multidimensional dynamics would involve an initially excited motion along *one* specific coordinate (described in a 1D friction model) followed by anharmonic coupling to a second mode relevant to the actual reaction. Here, the recent work by by Stépán et al.[51,74] on the femtosecond-laser-induced diffusion of O on a stepped Pt(111) surface serves as an instructive example. In addition to an extraordinarily high nonlinearity of the fluence dependence of the oxygen hopping probability, the authors report the two-pulse correlation of this hopping probability, which could not be described by a single constant frictional coefficient, η_{el}. However, if an empirical electronic temperature dependence of $\eta_{el}(T_{el})$ was assumed, the experimental data could be much better reproduced as illustrated in Figure 19, top panel, with a sketch of the experimental technique depicted in the inset. Two possible explanations for the temperature-dependent friction were given. Although, in principle, in accordance with Brandbyge's friction model (see section 2.2.), a high lying adsorbate resonance would exhibit such T_{el} dependence of η_{el}, there is experimental evidence that the unoccupied level for O/Pt(111) is rather broad and lies very close to the Fermi level.[142] Alternatively, if the adsorbate excitation occurs predominantly in a 1D scheme along the O−Pt stretch vibration followed by subsequent anharmonic coupling of this primary excitation coordinate to the effective reaction coordinate, that is, frustrated translation of the O atoms, the overall diffusion process would also appear strongly temperature dependent. The idea behind this anharmonic coupling between different modes whereby only one of them needs to be initially excited is schematically illustrated in the bottom part of Figure 19. Originally used to rationalize diffusion experiments of CO on Cu,[143] this picture is quite general and has been applied to various other systems, for example, refs 144 and 145. The primary electronic excitation occurs perpendicular to the surface plane, and after sufficient energy is accumulated

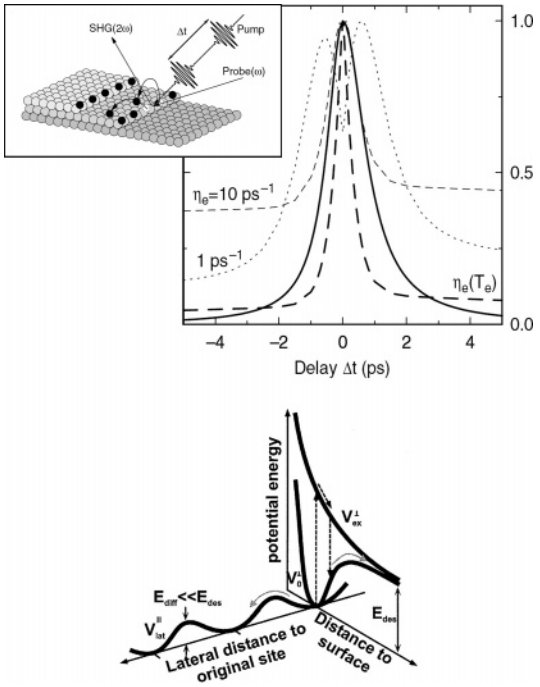

Figure 19. Anharmonic coupling between different modes (diffusion and desorption) in photostimulated diffusion studies of adsorbates on metal surfaces. (top) Femtosecond-laser excitation of the stepped Pt(111) surface induces diffusion of atomic O from step sites onto the terraces. Shown are a two-pulse correlation trace of the oxygen hopping rate in the experiment, solid line, together with various friction calculations based on constant electronic friction coefficients, thin dotted and dashed lines, and a temperature-dependent electronic friction, $\eta_{el}(T_{el})$, thick dashed line. Note that only the latter calculation comes close to the experimental results. This behavior was explained in terms of anharmonic coupling of the primary excited O−Pt stretch vibration to the frustrated translation essential for diffusion to occur. Reprinted with permission from *Phys. Rev. Lett.* (http://link.aps.org/abstract/PRL/v94/e236103), ref 51. Copyright 2005 American Physical Society. (bottom) Schematic two-dimensional potential energy diagram for electronic excitation of the adsorbate motion perpendicular and parallel to the surface plane. Electronic excitation−de-excitation cycles initially cause vibrational motion perpendicular to the surface plane, which subsequently couples energy into the diffusion coordinate. Reprinted from ref 143, Copyright 1998 with permission from Elsevier.

along this coordinate, anharmonic coupling to the orthogonal lateral coordinate enables the system to overcome the diffusion barrier. Finally, we note that in preliminary multidimensional friction calculations for the O/Pt system by Luntz and Persson,[146] neither temperature-dependent nor highly anisotropic electronic frictions were found so far, leaving the detailed mechanism encountered in the experiment for the femtosecond-laser-induced O diffusion on Pt unresolved.

6.2. Surface Femtochemistry and Impact on Related Fields

Nonadiabatic coupling between electronic and nuclear degrees of freedom as discussed in this review is of general importance in chemical reaction dynamics.[5,8] As such, surface femtochemistry is just one subfield of surface reaction dynamics where nonadiabaticity plays a crucial role. A main advantage of surface femtochemistry is the access to nonadiabatic coupling effects directly in the time domain, which allows one to "switch on" electronic frictional forces by an

ultrashort laser pulse. Such a pulse may also serve as an ultrafast trigger for real-time studies of surface reaction dynamics (see section 5.7. "Real-Time Studies"). The elementary mechanisms underlying surface femtochemistry have also many consequences for other fields. There is obviously a very close connection to nonadiabatic processes in gas−surface interactions where in exothermic adsorption reactions electron−hole pair excitation in the substrate leads to chemicurrents, chemiluminescense, or exoelectron emission.[6−8] These kinds of nonadiabatic processes in adsorption can be regarded (at least in part) as the time-reversal of DIET or DIMET processes in desorption. Recently, molecular beam experiments with state-selected highly vibrationally excited NO molecules with vibrational quanta $v \leq 18$ by Wodtke and co-workers[147−149] have shown a pronounced direct coupling of such large amplitude vibrational motions to electronic excitations in the metal substrate. The experimental signatures of this strong nonadiabatic (electron−vibrational) coupling are the unprecedented multiquantum vibrational energy relaxation[147,148] as well as the emission of energetic exoelectrons, which is 10^4 times more efficient than that observed in systems without large amplitude vibrations.[149] Because this area has already been reviewed comprehensively,[6−8] it will not be discussed in further detail here.

One particular field with a direct mechanistic link to surface femtochemistry is chemical reactions and electronic processes of single molecules induced by tunneling electrons or the electric field in a scanning tunneling microscopy (STM) configuration.[150−152] Low-temperature STM (temperatures typically <15 K) allows the imaging, excitation, and manipulation of individual molecules adsorbed on surfaces, while competing thermally activated processes such as diffusion are frozen out. Due to the ability to confine an excitation to a single bond or molecular group, STM has the potential for bond-selective "angstrochemistry".[150] In conjunction with inelastic tunneling spectroscopy, it provides an extremely powerful tool to study elementary processes on a single-molecule level.[151,153] We will briefly discuss several examples that demonstrate elementary processes closely related to surface femtochemistry, like nonlinear excitation via multiple inelastic transitions and anharmonic coupling between different vibrational modes.

An early demonstration for bond-selective chemistry with tunneling electrons was given by Stipe et al. for O_2/Pt(111).[154] Oxygen adsorbs molecularly on Pt(111) at temperatures below 100 K, which is accompanied by charge transfer from the substrate into an antibonding molecular resonance and weakening of the O−O bond.[155] At low temperatures, dissociation of individual molecules can be induced by inelastic tunneling of energetic electrons into the antibonding molecular resonance. The underlying mechanism is revealed by measuring the dissociation rate as a function of bias voltage and tunneling current (see Figure 20, top panel). The dissociation rate as a function of the tunneling current follows a power law dependence $R_d \propto I^n$, with $n = 0.8 \pm 0.2$, 1.8 ± 0.2, and 2.9 ± 0.3 for an applied bias voltage ΔV of 0.4, 0.3, and 0.2 V, respectively. This strongly supports a reaction mechanism by inelastic tunneling and vibrational ladder climbing as illustrated in bottom panel of Figure 20.[150,154] For dissociation of individual O_2 molecules, vibrational excitation of the O−O bond must exceed the activation barrier E_{diss} of 0.35−0.38 eV, which requires at least five vibrational quanta (in total ~0.4 eV). Since in the STM

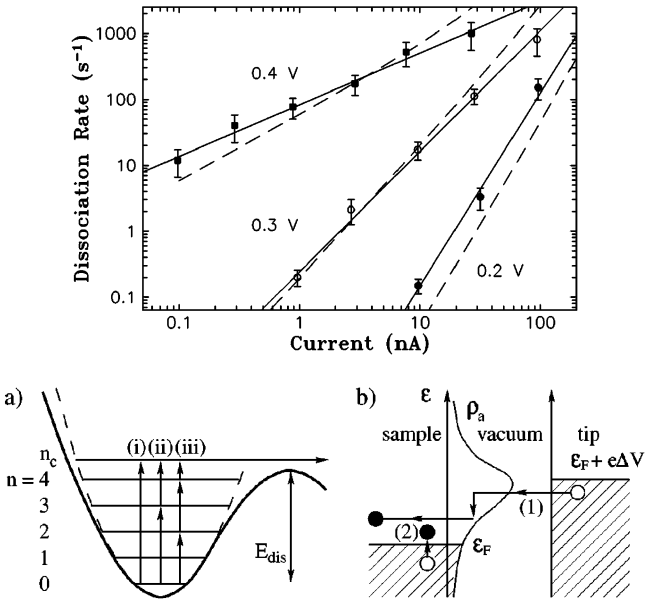

Figure 20. Electron-induced dissociation of a single O_2 molecule on Pt(111) via inelastic tunneling from the STM tip to the adsorbate-covered substrate. (top) Dissociation rate as a function of the tunneling current for applied biases ΔV of 0.4, 0.3, and 0.2 V. Least-squares fits $R_d \propto I^n$, solid lines, to the data yield power law exponents that are close to single (i), double (ii), and triple (iii) excitations explained in the bottom panel. (bottom) Schematic diagram of the model for the bond breaking of a single O_2 molecule. (a) PES for the intramolecular O−O stretching coordinate, solid line, which is approximated by a modeled truncated harmonic oscillator potential, dashed line. Arrows indicate typical transitions (i−iii), which lead to dissociation for various bias voltages ΔV identical to those of the top panel. (b) Inelastic electron tunneling to an adsorbate-induced resonance with density of states ρ_a creates vibrational excitations, process 1. Vibrational relaxation is accompanied by electron−hole pair excitations within the substrate, process 2. Reprinted with permission from *Phys. Rev. Lett.* (http://link.aps.org/abstract/PRL/v78/p4410), ref 154. Copyright 1997 American Physical Society.

experiment the rate of vibrational relaxation exceeds the excitation rate, the most likely pathway for dissociation is the one with the fewest transitions. Therefore, multiple inelastic scattering is required for a bias of 0.3 and 0.2 V (corresponding to a DIMET process in surface femtochemistry), while a single-scattering event is sufficient at $\Delta V = 0.4$ V (corresponding to a DIET scenario). Thus this work on O_2/Pt(111) by Stipe et al.[154] provides a beautiful demonstration for the crossover from the DIET to the DIMET regime in STM-induced reactions. It should be noted that in surface femtochemistry the high excitation density on a subpicosecond time scale usually leads to excitation rates that significantly exceed typical vibrational relaxation rates on metals. In this limit, the power law exponent n does not correspond to the minimum number of vibrational quanta necessary to break the chemical bond.[43,156] STM-induced processes in a similar regime have been also demonstrated, for example, for the transfer of Xe atoms between the surface and the tip ("atomic switch")[157] and the desorption of hydrogen atoms from silicon.[158] This again underlines the close mechanistic connection between STM-induced chemistry and surface femtochemistry.

More recent femtochemistry and STM experiments convincingly demonstrate the role of anharmonic coupling between different vibrational modes as a key mechanism for energy transfer from one preferentially excited coordinate to the reaction coordinate. As discussed already in section

6.1 ("Multidimensional Dynamics") for the femtosecond-laser-induced diffusion of atomic oxygen on a stepped Pt(111) surface by Stépán et al.,[51,74] the two-pulse correlation and the strong nonlinearity in the yield−fluence dependence have been explained in terms of anharmonic coupling of the primary excited O−Pt stretch vibration to the frustrated translation essential for diffusion to occur. Further examples of such anharmonic coupling effects are the lateral hopping of molecules induced by excitation of internal vibrational modes [CO on Pd(110)][144] and the mode selectivity in vibrationally mediated single-molecule chemistry [NH_3 on Cu(100)].[145] Both experiments clearly demonstrate energy transfer by anharmonic coupling and pave the way for mode-selective chemistry of individual adsorbed molecules.

The universality of the basic mechanisms in surface femtochemistry and STM-induced processes suggests an extension to femtochemistry on the nanoscale, where changes of the electronic structure of nanoparticles crucially determine their optical response and reactivity.[159,160] The specific characteristic of photoinduced chemistry on nanometer-sized metal particles arises from the fact that the excited electrons in such a system are confined on this length scale. Besides the resulting field enhancement of the exciting laser due to plasmon oscillations in the nanoparticle, which may be exploited to control the reaction mechanism (see section 6.3 on "The Challenge: Control of Surface Reactions"), the confinement of the electrons has certain consequences for surface photochemistry. The generation of secondary hot electrons is significantly enhanced, which may contribute to photochemical conversion, that is, bond breaking and formation, and second, the cooling of the electron temperature after ultrashort-laser pulse heating is slowed considerably,[188] which makes photochemical reactions more probable.[160]

6.3. The Challenge: Control of Surface Reactions

One of the major goals in chemical reaction dynamics is to control the efficiency and the selectivity of specific reaction channels by external stimuli such as light, pH, or the electrochemical potential. For photostimulated reactions, two complementary approaches have been demonstrated. The concept of coherent control, first proposed by Brumer and Shapiro,[161−163] relies on the quantum mechanical interference between two (or multiple) excitation pathways to the same final state, which evolves to different product channels. Control of the branching ratio between these channels is achieved by the phase difference of light, which excites the interfering pathways in analogy to Young's double slit experiment. Therefore, coherent control requires a sufficiently long coherence time of the *electronic* polarization induced by the exciting light field. Coherent control has been successfully demonstrated for various gas-phase photoreactions[164,165] but also for photoinduced currents in solids[166−168] and very recently at metal surfaces.[169] A second approach to reaction control has been introduced by Tannor, Kosloff, and Rice[170] whereby the chemical reaction is steered by a temporarily shaped laser pulse (or pulse sequence), which stimulates transitions between different PESs. Employing a feedback loop and learning algorithm, the laser field can be optimized to preferentially induce a specific reaction pathway.[171,172] A prerequisite for such optimum control scheme is *vibrational* coherence in the relevant reaction coordinate although elements of coherent control (interfering excitation pathways) may be operative as well.

Despite remarkable progress of coherent or optimum control in gas and solution phase reactions,[172−175] a similar level of sophistication has not been achieved for surface reactions. In part, this originates from the ultrashort time scales of competing dephasing and energy relaxation processes for molecules adsorbed on (metal) surfaces leading to a rapid loss of electronic and vibrational coherence. Thus control of surface reactions by light still remains a challenge. However, several attempts and concepts to control surface femtochemistry should be mentioned here:

(i) A very robust and generally applicable concept to discriminate between different reaction pathways exploits the time scales of different reaction mechanisms induced by direct excitation, hot substrate electrons, and phonons (see section 2.2. "Substrate−Adsorbate Coupling"). The femtosecond-laser-induced CO oxidation and desorption on Ru(0001) provides a good example of this type of (incoherent) reaction control.[17] While the $CO + O \rightarrow CO_2$ reaction is driven by ultrafast coupling to the hot photoexcited substrate electrons (see Figure 10), the competing reaction pathway of CO desorption is induced by coupling to the substrate temperature on a time scale where electrons and phonons have already equilibrated.[37] The branching ratio between both reaction channels thus depends critically on the temporal width of the excitation pulse (or pulse sequence), which can be used to control and optimize this ratio. However, this is feasible only within certain limits given by the finite time scale for electron thermalization and coupling to phonons, as well as practical aspects such as the damage threshold of the sample and the available laser pulse width.

(ii) The concept of reaction control via the time scale of the excitation mechanism can, in principle, be extended to direct excitation of the adsorbate by the driving laser field. The latter process is directly connected to the temporal shape of the laser pulse and allows exploitation of the phase of light for reaction control. Because this channel is effectively quenched for most reactions on (flat) metal surfaces, enhancement of the light field at nanostructured surfaces due to plasmon excitation has been proposed.[159,176,177] However, resonant excitation of metal nanoparticles results also in efficient heating of the particles, which may lead to thermal (phonon-mediated) desorption of the adsorbate and has been shown for desorption of water from quartz-supported Ag nanometer-sized clusters.[176] So far no successful experiments to control surface femtochemistry utilizing the field enhancement at nanostructured surfaces have been reported.

(iii) A rare example of direct excitation of the adsorbate−surface bond was given by Petek and co-workers for Cs/Cu(111).[22,111,112] Promotion of a single electron into the antibonding Cs 6s resonance by a femtosecond-laser pulse launches a vibrational wave packet motion of the Cs atom away from the surface. However, this motion is strongly damped, and no desorption has been observed so far (at least with a significant cross section). This work has been extended by Watanabe et al.[178−180] to coherent phonon excitation of alkali metals (Cs, K) on Pt(111) at higher fluences. Using sequential excitation by a pulse sequence provides some control of the amplitude of the adsorbate−surface stretch vibration.[180] However, anharmonic coupling to other modes, enhanced damping at high fluences, and the rather high energy barrier toward desorption hinder the application of an optimum control scheme to this system. Nevertheless, the latter work indicates a route to control surface femtochemistry by inducing vibrational coherent wave packet motion

of the reactants and optimizing the shape of the excitation pulse by feedback algorithms.

7. Conclusions

Surface femtochemistry on metal surfaces is based on electronically nonadiabatic coupling between a femtosecond-laser-excited distribution of electron−hole pairs in the substrate and adsorbate vibrational degrees of freedom. The resulting vibrational excitation eventually leads to chemical processes such as desorption, diffusion, or reactions between coadsorbed species. In contrast to conventional, thermally activated processes where the adsorbate degrees of freedom are nearly equilibrated with the substrate phonons, a reaction induced by femtosecond-laser excitation can be described by direct frictional coupling to an ultrafast electronic transient, which exceeds the lattice temperature by several thousand kelvin. Such a process violates the Born−Oppenheimer approximation and thus provides a test case to study the role of nonadiabaticity in surface reaction dynamics.

In the present paper, we have reviewed the basic experimental and theoretical concepts of surface femtochemistry at metal surfaces and provided a comprehensive overview of previous work and the current status of the field. The vast majority of all systems investigated so far can be successfully described within a 1D frictional model with a single adsorbate degree of freedom, although at least for bimolecular reactions multidimensional reaction dynamics are expected. Recent theoretical modeling of such a multidimensional association reaction with electronic frictions in conjunction with detailed experimental analysis of the energy partitioning provide a concept to disentangle the influence of (anisotropic) frictional forces and the dynamics governed by forces on the ground-state multidimensional PES. Depending on the anharmonicity and time scales of energy exchange between different adsorbate degrees of freedom, the reaction dynamics may be dominated by excitation of a particular mode (eventually followed by anharmonic coupling to other, for example, diffusional, modes) or by rapid thermalization on the ground-state PES. The concept of multidimensional dynamics with electronic frictions provides a simple and appealing approach to extend the established foundations of chemical reaction dynamics on Born−Oppenheimer surfaces to include nonadiabatic coupling to a hot electron transient. So far friction models have proven to be very robust and successful in surface femtochemistry and related fields despite the highly nonequilibrium excitation conditions. However, because the theory of molecular dynamics with friction relies on the approximation of "weak coupling", a new question arises: When does the frictional approach break down? There is obviously more to explore in the field of non-Born−Oppenheimer reactivity for both experiment and theory.

8. Acknowledgments

The authors would like to thank many co-workers, in particular Stephan Funk, Mischa Bonn, Christian Hess, Daniel Denzler, and Steffen Wagner for their key contributions to various parts of the work reviewed here. Also the successful collaborations with Marco Rutkowski and Helmut Zacharias as well as with Alan C. Luntz and Mats Persson are gratefully acknowledged. Gerhard Ertl deserves our special thanks for many fruitful discussions and his generous and continuous support. Finally, financial support by the Deutsche Forschungsgemeinschaft (DFG), especially through Sfb 450 "Analysis and control of ultrafast photoinduced reactions" is greatly appreciated.

9. References

(1) Zewail, A. H. *Femtochemistry−Ultrafast dynamics of the chemical bond*; World Scientific: Singapore, 1994.
(2) Zewail, A. H. *J. Phys. Chem. A* **2000**, *104*, 5660.
(3) Eyring, H. *Chem. Phys.* **1935**, *3*, 786.
(4) Evans, M. G.; Polanyi, M. *Trans. Faraday Soc.* **1935**, *31*, 875.
(5) Worth, G. A.; Cederbaum, L. S. *Annu. Rev. Phys. Chem.* **2004**, *55*, 127.
(6) Wodtke, A. M.; Tully, J. C.; Auerbach, D. J. *Int. Rev. Phys. Chem.* **2004**, *23*, 513.
(7) Greber, T. *Surf. Sci. Rep.* **1997**, *28*, 3.
(8) Nienhaus, H. *Surf. Sci. Rep.* **2002**, *45*, 3.
(9) Persson, B. N. J.; Persson, M. *Solid State Commun.* **1980**, *36*, 175.
(10) Diekhöner, L.; Hornekaer, L.; Mortensen, H.; Jensen, E.; Baurichter, A.; Petrunin, V. V.; Luntz, A. C. *J. Chem. Phys.* **2002**, *117*, 5018.
(11) Cavanagh, R. R.; King, D. S.; Stephenson, J. C.; Heinz, T. F. *J. Phys. Chem.* **1993**, *97*, 786.
(12) Anisimov, S. I.; Kapeliovich, B. L.; Perel'man, T. L. *Sov. Phys. JETP* **1974**, *39*, 375.
(13) Budde, F.; Heinz, T. F.; Loy, M. M. T.; Misewich, J. A.; Derougemont, F.; Zacharias, H. *Phys. Rev. Lett.* **1991**, *66*, 3024.
(14) Misewich, J. A.; Kalamarides, A.; Heinz, T. F.; Höfer, U.; Loy, M. M. T. *J. Chem. Phys.* **1994**, *100*, 736.
(15) Kao, F. J.; Busch, D. G.; Dacosta, D. G.; Ho, W. *Phys. Rev. Lett.* **1993**, *70*, 4098.
(16) Her, T. H.; Finlay, R. J.; Wu, C.; Mazur, E. *J. Chem. Phys.* **1998**, *108*, 8595.
(17) Bonn, M.; Funk, S.; Hess, C.; Denzler, D. N.; Stampfl, C.; Scheffler, M.; Wolf, M.; Ertl, G. *Science* **1999**, *285*, 1042.
(18) Denzler, D. N.; Frischkorn, C.; Wolf, M.; Ertl, G. *J. Phys. Chem. B* **2004**, *108*, 14503.
(19) Misewich, J. A.; Heinz, T. F.; Weigand, P.; Kalamarides, A. In *Laser Spectroscopy and Photochemistry on Metal Surfaces*; Dai, H.-L., Ho, W., Eds.; World Scientific: Singapore, 1995; Vol. 2.
(20) Zimmermann, F. M.; Ho, W. *Surf. Sci. Rep.* **1995**, *22*, 129.
(21) Al-Shamery, K.; Freund, H. J. *Curr. Opin. Solid State Mater. Sci.* **1996**, *1*, 622.
(22) Petek, H.; Ogawa, S. *Annu. Rev. Phys. Chem.* **2002**, *53*, 507.
(23) Prybyla, J. A.; Heinz, T. F.; Misewich, J. A.; Loy, M. M. T.; Glownia, J. H. *Phys. Rev. Lett.* **1990**, *64*, 1537.
(24) Groeneveld, R. H. M.; Sprik, R.; Lagendijk, A. *Phys. Rev. B* **1992**, *45*, 5079.
(25) Juhasz, T.; Elsayedali, H. E.; Smith, G. O.; Suarez, C.; Bron, W. E. *Phys. Rev. B* **1993**, *48*, 15488.
(26) Kaganov, M. I.; Lifshitz, I. M.; Tanatarov, L. V. *Sov. Phys. JETP* **1957**, *31*, 232.
(27) Anisimov, S. I.; Rethfeld, B. *Proc. SPIE* **1997**, *3093*, 192.
(28) Note that a linear heat capacity variation with T_{el} is valid only if the density of states of the metal substrate can be considered as flat over the relevant range of energies. However, this might not be an appropriate approximation for high temperatures in a material like Pd with a strongly peaked density of states around the Fermi level (Heinz, T. F., private communication).
(29) Kittel, C. *Introduction to Solid State Physics*; Wiley: New York, 2004.
(30) Ashcroft, N. W.; Mermin, N. D. *Solid State Physics*; Saunders College: Philadelphia, PA, 1988.
(31) Fann, W. S.; Storz, R.; Tom, H. W. K.; Bokor, J. *Phys. Rev. Lett.* **1992**, *68*, 2834.
(32) Fann, W. S.; Storz, R.; Tom, H. W. K.; Bokor, J. *Phys. Rev. B* **1992**, *46*, 13592.
(33) Papaconstantopoulus, D. A. *Handbook of the band structure of elemental solids*; Plenum Press: New York, 1986.
(34) Deliwala, S.; Finlay, R. J.; Goldman, J. R.; Her, T. H.; Mieher, W. D.; Mazur, E. *Chem. Phys. Lett.* **1995**, *242*, 617.
(35) Lisowski, M.; Loukakos, P. A.; Bovensiepen, U.; Stähler, J.; Gahl, C.; Wolf, M. *Appl. Phys. A* **2004**, *78*, 165.
(36) Note that ballistic electron transport has been included in the 2TM also by using an increased optical penetration depth. See Hohlfeld, J.; Wellershoff, S.-S.; Güdde, J.; Conrad, U.; Jähnke, V.; Matthias, E. *Chem. Phys.* **2000**, *251*, 237.
(37) Funk, S.; Bonn, M.; Denzler, D. N.; Hess, C.; Wolf, M.; Ertl, G. *J. Chem. Phys.* **2000**, *112*, 9888.
(38) Denzler, D. N.; Frischkorn, C.; Hess, C.; Wolf, M.; Ertl, G. *Phys. Rev. Lett.* **2003**, *91*, 226102.
(39) Budde, F.; Heinz, T. F.; Kalamarides, A.; Loy, M. M. T.; Misewich, J. A. *Surf. Sci.* **1993**, *283*, 143.

(40) Brandbyge, M.; Hedegard, P.; Heinz, T. F.; Misewich, J. A.; Newns, D. M. *Phys. Rev. B* **1995**, *52*, 6042.
(41) Tully, J. C.; Gomez, M.; Head-Gordon, M. *J. Vac. Sci. Technol. A* **1993**, *11*, 1914.
(42) Newns, D. M. *Phys. Rev.* **1969**, *178*, 1123.
(43) Misewich, J. A.; Heinz, T. F.; Newns, D. M. *Phys. Rev. Lett.* **1992**, *68*, 3737.
(44) Menzel, D.; Gomer, R. *J. Chem. Phys.* **1964**, *41*, 3311.
(45) Redhead, P. A. *Can. J. Phys.* **1964**, *42*, 886.
(46) Antoniewicz, P. R. *Phys. Rev. B* **1980**, *21*, 3811.
(47) Newns, D. M.; Heinz, T. F.; Misewich, J. A. *Prog. Theor. Phys.* **1991**, *106*, 411.
(48) Struck, L. M.; Richter, L. J.; Buntin, S. A.; Cavanagh, R. R.; Stephenson, J. C. *Phys. Rev. Lett.* **1996**, *77*, 4576.
(49) Note that the symbol η is used by some authors (e.g., Luntz, A. C.; Persson, M. *J. Chem. Phys.* **2005**, *123*, 074704) for the mass-independent electronic friction coefficients. In their notation, $\gamma = \eta/m$ describes the mass-dependent damping rate corresponding to the coefficient η introduced here.
(50) Güdde, J.; Höfer, U. *J. Phys.: Condens. Matter* **2006**, *18*, S1409.
(51) Stépán, K.; Güdde, J.; Höfer, U. *Phys. Rev. Lett.* **2005**, *94*, 236103.
(52) Wagner, S.; Frischkorn, C.; Wolf, M.; Rutkowski, M.; Zacharias, H.; Luntz, A. C. *Phys. Rev. B* **2005**, *72*, 205404.
(53) Luntz, A. C.; Persson, M.; Wagner, S.; Frischkorn, C.; Wolf, M. *J. Chem. Phys.* **2006**, *124*, 244702.
(54) Wetzig, D.; Rutkowski, M.; Zacharias, H.; Gross, A. *Phys. Rev. B* **2001**, *63*, 205412.
(55) Lichtman, D.; Shapira, Y. *CRC Crit. Rev. Solid State Mater. Sci.* **1978**, *8*, 93.
(56) Zhou, X.-L.; Zhu, X.-Y.; White, J. M. *Surf. Sci. Rep.* **1991**, *13*, 73.
(57) Frischkorn, C. *Surf. Sci.* **2005**, *593*, 67.
(58) Bartels, L.; Wang, F.; Moller, D.; Knoesel, E.; Heinz, T. F. *Science* **2004**, *305*, 648.
(59) Backus, E. H. G.; Eichler, A.; Kleyn, A. W.; Bonn, M. *Science* **2005**, *310*, 1790.
(60) Bonn, M.; Hess, C.; Funk, S.; Miners, J. H.; Persson, B. N. J.; Wolf, M.; Ertl, G. *Phys. Rev. Lett.* **2000**, *84*, 4653.
(61) Head-Gordon, M.; Tully, J. C. *Surf. Sci.* **1994**, *320*, L57.
(62) Head-Gordon, M.; Tully, J. C. *J. Chem. Phys.* **1995**, *103*, 10137.
(63) Luntz, A. C.; Persson, M. *J. Chem. Phys.* **2005**, *123*, 074704.
(64) Denzler, D. N.; Hess, C.; Funk, S.; Ertl, G.; Bonn, M.; Frischkorn, C.; Wolf, M. In *Femtochemistry and Femtobiology—Ultrafast Dynamics in Molecular Science*; Douhal, A., Santamaria, J., Eds.; World Scientific: Singapore, 2002.
(65) Kao, F. J.; Busch, D. G.; Cohen, D.; Dacosta, D. G.; Ho, W. *Phys. Rev. Lett.* **1993**, *71*, 2094.
(66) Yamanaka, T.; Hellman, A.; Gao, S. W.; Ho, W. *Surf. Sci.* **2002**, *514*, 404.
(67) Finlay, R. J.; Her, T. H.; Wu, C.; Mazur, E. *Chem. Phys. Lett.* **1997**, *274*, 499.
(68) Busch, D. G.; Ho, W. *Phys. Rev. Lett.* **1996**, *77*, 1338.
(69) Misewich, J. A.; Nakabayashi, S.; Weigand, P.; Wolf, M.; Heinz, T. F. *Surf. Sci.* **1996**, *363*, 204.
(70) Symonds, J. P. R.; Arnolds, H.; King, D. A. *J. Phys. Chem. B* **2004**, *108*, 14311.
(71) Fournier, F.; Zheng, W.; Carrez, S.; Dubost, H.; Bourguignon, B. *J. Chem. Phys.* **2004**, *121*, 4839.
(72) Berthold, W.; Feulner, P.; Höfer, U. *Surf. Sci.* **2004**, *548*, L13.
(73) Bauer, M.; Lei, C.; Read, K.; Tobey, R.; Gland, J.; Murnane, M. M.; Kapteyn, H. C. *Phys. Rev. Lett.* **2001**, *8702*, 025501.
(74) Stépán, K.; Dürr, M.; Güdde, J.; Höfer, U. *Surf. Sci.* **2005**, *593*, 54.
(75) Madey, T. E. *Science* **1986**, *234*, 316.
(76) Alternatively, the translational energy derived from TOF spectra as a function of the pulse−pulse delay can be used to demonstrate the underlying energy transfer mechanism as demonstrated by Busch et al. (Busch, D. G.; Gao, S.; Pelak, R. A.; Booth, M. F.; Ho, W. *Phys. Rev. Lett.* **1995**, *75*, 673) for O_2 desorption from Pt(111). Moreover, Stépán et al. (Stépán, K.; Güdde, J.; Höfer, U. *Phys. Rev. Lett.* **2005**, *94*, 236103 and Stépán, K.; Dürr, M.; Güdde, J.; Höfer, U. *Surf. Sci.* **2005**, *593*, 54) applied second harmonic generation (SHG) as a very sensitive probe of femtosecond-laser-induced diffusion of O on Pt-(111) as a function of the pulse−pulse separation.
(77) Germer, T. A.; Stephenson, J. C.; Heilweil, E. J.; Cavanagh, R. R. *J. Chem. Phys.* **1994**, *101*, 1704.
(78) Cai, L.; Xiao, X. D.; Loy, M. M. T. *Surf. Sci.* **2001**, *492*, L688.
(79) Dudek, R.; Wolf, M.; Frischkorn, C. Manuscript in preparation.
(80) Bonn, M.; Denzler, D. N.; Funk, S.; Wolf, M.; Wellershoff, S. S.; Hohlfeld, J. *Phys. Rev. B* **2000**, *61*, 1101.
(81) Cai, L.; Xiao, X. D.; Loy, M. M. T. *Surf. Sci.* **2000**, *464*, L727.
(82) Micha, D. A.; Yi, Z. *Chem. Phys. Lett.* **1998**, *298*, 250.
(83) Yata, M.; Madix, R. J. *Surf. Sci.* **1995**, *328*, 171.
(84) Menzel, D. *Surf. Sci.* **1975**, *47*, 370.
(85) Wagner, S.; Öström, H.; Kaebe, A.; Krenz, M.; Wolf, M.; Luntz, A. C.; Frischkorn, C. Manuscript in preparation.
(86) Rendulic, K. D.; Anger, G.; Winkler, A. *Surf. Sci.* **1989**, *208*, 404.
(87) Gross, A.; Wilke, S.; Scheffler, M. *Phys. Rev. Lett.* **1995**, *75*, 2718.
(88) Michelsen, H. A.; Auerbach, D. J. *J. Chem. Phys.* **1991**, *94*, 7502.
(89) McCormack, D. A.; Kroes, G. J.; Olsen, R. A.; Groeneveld, J. A.; van Stralen, J. N. P.; Baerends, E. J.; Mowrey, R. C. *Faraday Discuss.* **2000**, 109.
(90) Hammer, B.; Scheffler, M.; Jacobsen, K. W.; Nørskov, J. K. *Phys. Rev. Lett.* **1994**, *73*, 1400.
(91) Eyring, H.; Polanyi, M. *Z. Phys. Chem. B* **1931**, *12*, 279.
(92) Eichhorn, G.; Richter, M.; Al-Shamery, K.; Zacharias, H. *Surf. Sci.* **1996**, *368*, 67.
(93) The same considerations on flux vs density distributions of the desorbing particles also apply to experiments in which the ionization of desorption product is achieved by the REMPI method in the laser focus. This kind of studies, for example, Struck, L. M.; Richter, L. J.; Buntin, S. A.; Cavanagh, R. R.; Stephenson, J. C. *Phys. Rev, Lett.* **1996**, *77*, 4576, allows in addition determination of the energy partitioning into internal degrees of freedom due to the state selectivity of this ionization technique (see section 5.5.2).
(94) Hasselbrink, E. In *Laser spectroscopy and photochemistry on metal surfaces*; Dai, H.-L., Ho, W., Eds.; World Scientific: Singapore, 1995.
(95) Comsa, G.; David, R. *Surf. Sci. Rep.* **1985**, *5*, 145.
(96) If the mean translational energy is calculated in a theoretical model based on a single translational degree of freedom, the appropriate translational temperature is then $T_{trans} = \langle E_{trans} \rangle / k_B$. In contrast, typical experiments measure the component of the translational energy normal to the (two-dimensional) surface resulting in an $\langle E_{trans} \rangle$ twice as high as in the one-dimensional model; hence the factor of 2 (see Luntz, A. C.; Persson, M.; Wagner, S.; Frischkorn, C.; Wolf, M. *J. Chem. Phys.* **2006**, *124*, 244702).
(97) Cowin, J. P.; Auerbach, D. J.; Becker, C.; Wharton, L. *Surf. Sci.* **1978**, *78*, 545.
(98) Feulner, P.; Menzel, D. *Surf. Sci.* **1985**, *154*, 465.
(99) Vincent, J. K.; Olsen, R. A.; Kroes, G. J.; Luppi, M.; Baerends, E. J. *J. Chem. Phys.* **2005**, *122*, 044701.
(100) Luppi, M.; Olsen, R. A.; Baerends, E. J. Unpublished.
(101) Zacharias, H. *Int. J. Mod. Phys. B* **1990**, *4*, 45.
(102) Greene, C. H.; Zare, R. N. *Annu. Rev. Phys. Chem.* **1982**, *33*, 119.
(103) Rutkowski, M.; Wetzig, D.; Zacharias, H.; Gross, A. *Phys. Rev. B* **2002**, *66*, 115405.
(104) Schröter, L.; Zacharias, H.; David, R. *Phys. Rev. Lett.* **1989**, *62*, 571.
(105) Bratu, P.; Höfer, U. *Phys. Rev. Lett.* **1995**, *74*, 1625.
(106) Kolasinski, K. W.; Nessler, W.; de Meijere, A.; Hasselbrink, E. *Phys. Rev. Lett.* **1994**, *72*, 1356.
(107) Brenig, W.; Gross, A.; Russ, R. *Z. Phys. B* **1994**, *96*, 231.
(108) Dürr, M.; Raschke, M. B.; Höfer, U. *J. Chem. Phys.* **1999**, *111*, 10411.
(109) Sagara, T.; Kuga, T.; Tanaka, K.; Shibataka, T.; Fujimoto, T.; Namiki, A. *Phys. Rev. Lett.* **2002**, *89*, 086101.
(110) Shibataka, T.; Matsuno, T.; Tsurumaki, H.; Namiki, A. *Phys. Rev. B* **2003**, *68*, 113307.
(111) Petek, H.; Weida, M. J.; Nagano, H.; Ogawa, S. *Science* **2000**, *288*, 1402.
(112) Petek, H.; Nagano, H.; Weida, M. J.; Ogawa, S. *J. Phys. Chem. B* **2001**, *105*, 6767.
(113) Hand, M.; Harris, J. *J. Chem. Phys.* **1990**, *92*, 7610.
(114) Watanabe, K.; Matsumoto, Y. Private communication.
(115) Murphy, M. J.; Skelly, J. F.; Hodgson, A.; Hammer, B. *J. Chem. Phys.* **1999**, *110*, 6954.
(116) Diekhöner, L.; Mortensen, H.; Baurichter, A.; Luntz, A. C.; Hammer, B. *Phys. Rev. Lett.* **2000**, *84*, 4906.
(117) Klamroth, T.; Saalfrank, P. Private communication.
(118) Lindroos, M.; Pfnür, H.; Menzel, D. *Surf. Sci.* **1987**, *192*, 421.
(119) *The chemical physics of solid surfaces—Coadsorption, promoters and poisons*; King, D. A., Woodruff, D. P., Eds.; Elsevier: Amsterdam, 1993.
(120) Bird, D. *Faraday Discuss.* **1998**, *110*, 335.
(121) Hammer, B.; Norskov, J. K. *Adv. Catal.* **2000**, *45*, 71.
(122) Greuter, R. G.; Strathy, I.; Plummer, E. W.; Eberhardt, W. *Phys. Rev. B* **1986**, *33*, 736.
(123) Mitsui, T.; Rose, M. K.; Fomin, E.; Ogletree, D. F.; Salmeron, M. *Nature* **2003**, *422*, 705.
(124) Fournier, F.; Zheng, W.; Carrez, S.; Dubost, H.; Bourguignon, B. *Phys. Rev. Lett.* **2004**, *92*, 216102.
(125) Fournier, F.; Zheng, W.; Carrez, S.; Dubost, H.; Bourguignon, B. *Phys. Rev. Lett.* **2004**, *93*, 249602.
(126) Roeterdink, W. G.; Backus, E. H. G.; Kleyn, A. W.; Bonn, M. *Phys. Rev. Lett.* **2004**, *93*, 249601.
(127) Bonn, M. Private communication.
(128) Prybyla, J. A.; Tom, H. W. K.; Aumiller, G. D. *Phys. Rev. Lett.* **1992**, *68*, 503.

(129) Bandara, A.; Kubota, J.; Onda, K.; Wada, A.; Kano, S. S.; Domen, K.; Hirose, C. *J. Phys. Chem. B* **1998**, *102*, 5951.
(130) Bandara, A.; Kubota, J.; Wada, A.; Domen, K.; Hirose, C. *Appl. Phys. B* **1999**, *68*, 573.
(131) Kubota, J.; Wada, A.; Kano, S. S.; Domen, K. *Chem. Phys. Lett.* **2003**, *377*, 217.
(132) Kubota, J.; Yoda, E.; Ishizawa, N.; Wada, A.; Domen, K.; Kano, S. S. *J. Phys. Chem. B* **2003**, *107*, 10329.
(133) Kubota, J.; Wada, A.; Domen, K. *J. Phys. Chem. B* **2005**, *109*, 20973.
(134) Richter, L. J.; Petralli-Mallow, T. P.; Stephenson, J. C. *Opt. Lett.* **1998**, *23*, 1594.
(135) Roke, S.; Kleyn, A. W.; Bonn, M. *J. Phys. Chem. A* **2001**, *105*, 1683.
(136) Backus, E. H. G.; Bonn, M. *Chem. Phys. Lett.* **2005**, *412*, 152.
(137) Ueba, H.; Wolf, M. *Science* **2005**, *310*, 1774.
(138) Ranea, V. A.; Michaelides, A.; Ramirez, R.; de Andres, P. L.; Verges, J. A.; King, D. A. *Phys. Rev. Lett.* **2004**, *92*, 136104.
(139) Hellsing, B.; Persson, M. *Phys. Scr.* **1984**, *29*, 360.
(140) Trail, J. R.; Bird, D.; Persson, M.; Holloway, S. *J. Chem. Phys.* **2003**, *119*, 4539.
(141) Tully, J. C. *J. Chem. Phys.* **1980**, *73*, 1975.
(142) Puglia, C.; Nilsson, A.; Hernnäs, B.; Karis, O.; Bennich, P.; Martensson, N. *Surf. Sci.* **1995**, *342*, 119.
(143) Bartels, L.; Wolf, M.; Meyer, G.; Rieder, K.-H. *Chem. Phys. Lett.* **1998**, *291*, 573.
(144) Komeda, T.; Kim, Y.; Kawai, M.; Persson, B. N. J.; Ueba, H. *Science* **2002**, *295*, 2055.
(145) Pascual, J. I.; Lorente, N.; Song, Z.; Conrad, H.; Rust, H. P. *Nature* **2003**, *423*, 525.
(146) Luntz, A. C.; Persson, M. Manuscript in preparation.
(147) Hou, H.; Huang, Y.; Gulding, S. J.; Rettner, C. T.; Auerbach, D. J.; Wodtke, A. M. *Science* **1999**, *284*, 1647.
(148) Huang, Y. H.; Rettner, C. T.; Auerbach, D. J.; Wodtke, A. M. *Science* **2000**, *290*, 111.
(149) White, J. D.; Chen, J.; Matsiev, D.; Auerbach, D. J.; Wodtke, A. M. *Nature* **2005**, *433*, 503.
(150) Ho, W. *Acc. Chem. Res.* **1998**, *31*, 567.
(151) Ho, W. *J. Chem. Phys.* **2002**, *117*, 11033.
(152) Hla, S.-W.; Rieder, K.-H. *Annu. Rev. Phys. Chem.* **2003**, *54*, 307.
(153) Pascual, J. I. *Eur. Phys. J. D* **2005**, *35*, 327.
(154) Stipe, B. C.; Rezaei, M. A.; Ho, W.; Gao, S.; Persson, M.; Lundqvist, B. I. *Phys. Rev. Lett.* **1997**, *78*, 4410.
(155) Gland, J. L.; Sexton, B. A.; Fischer, G. B. *Surf. Sci.* **1980**, *95*, 587.
(156) Gadzuk, J. W. *Chem. Phys.* **2000**, *251*, 87.
(157) Eigler, D. M.; Lutz, C. P.; Rudge, W. E. *Nature* **1991**, *352*, 600.
(158) Avouris, P. *Acc. Chem. Res.* **1995**, *28*, 95.
(159) Watanabe, K.; Menzel, D.; Nilius, N.; Freund, H. J. *Chem. Rev.*, in press.
(160) Zhdanov, V. P.; Kasemo, B. *J. Phys.: Condens. Matter* **2004**, *16*, 7131.
(161) Shapiro, M.; Brumer, P. *J. Chem. Phys.* **1986**, *84*, 4103.
(162) Brumer, P.; Shapiro, M. *Chem. Phys. Lett.* **1986**, *126*, 541.
(163) Brumer, P.; Shapiro, M. *Annu. Rev. Phys. Chem.* **1992**, *43*, 257.
(164) Yian, Y.; Chen, C.; Elliot, D. S. *Phys. Rev. Lett.* **1992**, *69*, 2353.
(165) Zhu, L.; Kleiman, V.; Li, X.; Lu, S.; Trentelman, K.; Gordon, R. J. *Science* **1995**, *270*, 77.
(166) Atanasov, R.; Haché, A.; Hughes, J. L. P.; van Driel, H. M.; Sipe, J. E. *Phys. Rev. Lett.* **1996**, *76*, 1703.
(167) Haché, A.; Sipe, J. E.; van Driel, H. M. *IEEE J. Quantum Electron.* **1998**, *34*, 1144.
(168) Stevens, M. J.; Najmaie, A.; Bhat, R. D. R.; Sipe, J. E.; van Driel, H. M.; Smirl, A. L. *J. Appl. Phys.* **2003**, *94*, 4999.
(169) Güdde, J.; Rohleder, M.; Höfer, U. *Appl. Phys. A*, in press.
(170) Tannor, D. J.; Kosloff, R.; Rice, S. A. *J. Chem. Phys.* **1986**, *85*, 5805.
(171) Judson, R. S.; Rabitz, H. *Phys. Rev. Lett.* **1992**, *68*, 1500.
(172) Rabitz, H.; de Vievie-Riedle, R.; Motzkus, M.; Kompa, K. *Science* **2000**, *288*, 824.
(173) Assion, A.; Baumert, T.; Bergt, M.; Brixner, T.; Kiefer, B.; Seyfried, V.; M., S.; Gerber, G. *Science* **1998**, *282*, 919.
(174) Daniel, C.; Full, J.; González, L.; Lupulescu, C.; Manz, J.; Merli, A.; Vajda, S.; Wöste, L. *Science* **2003**, *299*, 536.
(175) Brixner, T.; Damrauer, N. H.; Niklaus, P.; Gerber, G. *Nature* **2001**, *414*, 57.
(176) Kwiet, S.; Starr, D. E.; Grujic, A.; Wolf, M.; Hotzel, A. *Appl. Phys. B* **2005**, *80*, 115.
(177) Evers, F.; Rakete, C.; Watanabe, K.; Menzel, D.; Freund, H. J. *Surf. Sci.* **2005**, *593*, 43.
(178) Watanabe, K.; Takagi, N.; Matsumoto, Y. *Phys. Rev. Lett.* **2004**, *92*, 057401.
(179) Watanabe, K.; Takagi, N.; Matsumoto, Y. *Chem. Phys. Lett.* **2002**, *366*, 606.
(180) Watanabe, K.; Takagi, N.; Matsumoto, Y. *Phys. Chem. Chem. Phys.* **2005**, *7*, 2697.
(181) Busch, D. G.; Gao, S. W.; Pelak, R. A.; Booth, M. F.; Ho, W. *Phys. Rev. Lett.* **1995**, *75*, 673.
(182) Quinn, D. P.; Heinz, T. F. *J. Vac. Sci. Technol. A* **2003**, *21*, 1312.
(183) Arnolds, H. *Surf. Sci.* **2004**, *548*, 151.
(184) Arnolds, H.; Rehbein, C. E. M.; Roberts, G.; Levis, R. J.; King, D. A. *Chem. Phys. Lett.* **1999**, *314*, 389.
(185) Arnolds, H.; Rehbein, C.; Roberts, G.; Levis, R. J.; King, D. A. *J. Phys. Chem. B* **2000**, *104*, 3375.
(186) Fournier, F.; Zheng, W. Q.; Carrez, S.; Dubost, H.; Bourguignon, B. *Surf. Sci.* **2003**, *528*, 177.
(187) Hess, C.; Funk, S.; Bonn, M.; Denzler, D. N.; Wolf, M.; Ertl, G. *Appl. Phys. A* **2000**, *71*, 477.
(188) Bauer, C.; Abid, J. P.; Girault, H. H. *J. Phys. Chem. B* **2006**, *110*, 4519.

CR050161R